

UNIVERSITY OF OKLAHOMA
GRADUATE COLLEGE

INVESTIGATION OF A GENERALIZED FREQUENCY DOMAIN METHOD
FOR MODELING TIME-VARYING LOADS ON ANTENNAS

A THESIS
SUBMITTED TO THE GRADUATE FACULTY
in partial fulfillment of the requirements for the
Degree of
MASTER OF SCIENCE

By
ASHLEY PALMER
Norman, Oklahoma
2019

INVESTIGATION OF A GENERALIZED FREQUENCY DOMAIN METHOD
FOR MODELING TIME-VARYING LOADS ON ANTENNAS

A THESIS APPROVED FOR THE
SCHOOL OF ELECTRICAL AND COMPUTER ENGINEERING

BY THE COMMITTEE CONSISTING OF

Dr. Jessica Ruyle, Chair

Dr. Jay McDaniel

Dr. Justin Metcalf

© Copyright by ASHLEY PALMER 2019

All Rights Reserved.

Acknowledgments

I would like to thank my committee for all the guidance they have provided for the entirety of my graduate program. I would especially like to thank Dr. Ruyle for the mentorship she has given me during her time as my advisor. I am very fortunate to have an advisor that has followed me through the entirety of both my undergraduate and graduate degrees, and focused on not only my academic, but also professional development. The last couple years have been a compilation of long days and some late nights in the lab, and I am very grateful that I had such a wonderful group of friends to learn from and grow with as well.

My degree would also not have been possible without the constant support of my family, especially my parents. I am very appreciative that my degree allowed me extra years living so close to home, and will always be thankful for the good advice and free meals. I would like to conclude by thanking Andrew Cook for his encouragement and love throughout my graduate experience. While I have questioned my capability many times, he never did and made sure to remind me of that every day. I am very lucky to have the privilege to go through life with such a wonderful teammate.

Table of Contents

| | |
|--|-------------|
| Acknowledgment | iv |
| List of Figures | viii |
| Abstract | xiii |
| 1 Introduction | 1 |
| 2 Method of Moments | 7 |
| 2.1 Thin Wire Antenna Approximation | 8 |
| 2.1.1 Hallen and Pocklington Equations | 10 |
| 2.2 Basis Functions | 11 |
| 2.3 Antenna Analysis using Method of Moments | 15 |
| 2.3.1 Applying Loads | 16 |
| 2.3.2 Excitations | 18 |
| 2.4 Summary | 21 |
| 3 Landt Integral Method for Time-Varying Loads | 22 |
| 3.1 Integral Equation Basis | 22 |
| 3.2 Loaded Matrix Relations | 23 |
| 3.3 Results and Applications | 26 |
| 3.4 Summary | 27 |

| | | |
|----------|--|-----------|
| 4 | Introduction of Conversion Matrices | 29 |
| 4.1 | Background of Large-Signal/Small-Signal Analysis | 29 |
| 4.2 | Structure of Conversion Matrices | 30 |
| 4.2.1 | Excitations | 31 |
| 4.2.2 | Static Components | 31 |
| 4.2.3 | Time-Varying Components | 33 |
| 4.3 | Circuit Analysis with Conversion Matrices | 36 |
| 4.3.1 | Nodal Analysis | 39 |
| 4.4 | Summary | 41 |
| 5 | Conversion Matrices Antenna Applications | 42 |
| 5.1 | Past Conversion Matrix Antenna Application | 42 |
| 5.1.1 | Setbacks with Previous Work | 43 |
| 5.2 | Expansion to Harrington Method of Moments | 44 |
| 5.2.1 | Impedance Conversion Matrix | 45 |
| 5.2.2 | Loading the Conversion Matrix | 47 |
| 5.2.3 | Excitation Matrix | 50 |
| 5.3 | Current Distribution | 52 |
| 5.4 | Comparison of Performance | 54 |
| 5.4.1 | Base Results | 55 |
| 5.4.2 | Varying Locations | 57 |
| 5.4.3 | Multiple Loads | 58 |
| 5.5 | Summary | 60 |
| 6 | Generalization of the Conversion Matrices Method | 61 |
| 6.1 | Wire Meshing | 62 |
| 6.1.1 | Thin Wire Dipole | 62 |
| 6.2 | Planar Meshing | 70 |
| 6.2.1 | Ribbon Dipole | 74 |

| | |
|--------------------------------------|-----------|
| 6.3 Summary | 81 |
| 7 Conclusions and Future Work | 82 |
| References | 85 |

List of Figures

| | | |
|-----|--|----|
| 1.1 | Omni-direction antenna used to prove limitations of electrically small antennas from [2] | 2 |
| 1.2 | Visualization of proposed application of time-varying loads to antennas | 3 |
| 1.3 | Example of direct antenna modulation created by a switch from [10] | 4 |
| 1.4 | Equivalent circuit of antenna with modulated load from [22] | 6 |
| 2.1 | Model used for the thin wire antenna approximation from [26] | 10 |
| 2.2 | Accuracy of Hallen vs. Pocklington integral equations from [25] | 12 |
| 2.3 | Representation of delta basis function from [26] | 12 |
| 2.4 | Representation of pulse basis function from [26] | 13 |
| 2.5 | Representation of piecewise triangular basis function from [26] | 14 |
| 2.6 | Representation of piecewise NEC basis function from [26] | 14 |
| 2.7 | Figure representing antennas being loaded using multi-port system from [20] | 16 |
| 2.8 | Excitation models of delta-gap and plane wave source from [26] | 18 |
| 2.9 | Excitation model of magnetic frill source from [25] | 20 |
| 3.1 | Example of wire antenna with a time-varying Load | 26 |
| 3.2 | Results of E-field spectrum from [17] of provided example along with results of current spectrum from MATLAB code meant to replicate Landt example | 27 |

| | | |
|-----|--|----|
| 3.3 | Waveform of field vs. time from [17] and the result of current vs. time -from MATLAB code meant to replicate the example | 28 |
| 4.1 | Format of time-varying component conversion matrix along with excitation matrices from [23] | 30 |
| 4.2 | Mixing frequency representation from [23] | 32 |
| 4.3 | Format of static impedance conversion matrix from [23] | 32 |
| 4.4 | Omega conversion matrix for time-varying reactances from [23] | 36 |
| 4.5 | Example circuit to be solved with conversion matrices | 38 |
| 4.6 | Example circuit for conversion matrix analysis from [23] | 40 |
| 4.7 | Two node network from [23] | 40 |
| 4.8 | Nodal matrix for system of greater than two nodes from [23] | 40 |
| 5.1 | Equivalent circuit used by [22] to apply conversion matrices to antennas | 43 |
| 5.2 | Equivalent circuit used by [24] to describe capacitive switches on antenna | 43 |
| 5.3 | Example of wire antenna separated into three segments | 46 |
| 5.4 | Example of wire antenna now with the addition of a time-varying load | 49 |
| 5.5 | The current spectrum from the extracted conversion matrix | 55 |
| 5.6 | Result of current spectrum from Landt Integral Method and comparison to result from Conversion Matrices Method | 56 |
| 5.7 | Result of current waveform from both Landt Integral Method and Conversion Matrices Method | 56 |
| 5.8 | Visualization of an example used to test the results of differing feed locations using Conversion Matrices Method | 57 |
| 5.9 | Results from the Landt Integral Method and Conversion Matrices Method one segment away from the load | 58 |

| | | |
|------|---|----|
| 5.10 | Visualization of example used to test the results of multiple loads using the Conversion Matrices Method | 59 |
| 5.11 | Comparison of the Landt and Conversion Matrices methods for a dipole antenna with two time-varying resistances and single feed point all located at different locations | 59 |
| 6.1 | Representation of piecewise triangular basis function from [26] that is used by FEKO | 62 |
| 6.2 | Simulated model in FEKO for wire antenna, separated into 10 segments with 9 edges between segments | 64 |
| 6.3 | Setup of simulation done for FEKO extracted wire antenna impedance matrix with load and feed at the center of the dipole | 64 |
| 6.4 | Results of current spectrum on the central load from Landt Integral Method and Conversion Matrices Method using FEKO extracted impedance matrix of a wire antenna | 65 |
| 6.5 | Setup of simulation done for FEKO extracted wire antenna impedance matrix with load on the second edge between segments | 65 |
| 6.6 | Result of the current spectrum on the load from Landt Integral Method and Conversion Matrices Method using FEKO extracted impedance matrix of a wire antenna with the load moved to the second edge from the end of the antenna | 66 |
| 6.7 | Setup of simulation done for FEKO extracted wire antenna impedance matrix to test feed points away from the load | 66 |
| 6.8 | Result of current spectrum on the load from both methods using FEKO extracted impedance matrix of wire antenna to test feed points away from the load | 67 |
| 6.9 | Setup of simulation done for FEKO extracted wire antenna impedance matrix to test multiple loads | 68 |

| | | |
|------|---|----|
| 6.10 | Result of current spectrum on the load from both methods using FEKO extracted impedance matrix of wire antenna to test multiple loads | 68 |
| 6.11 | Result of current spectrum on wire antenna with higher f_s to avoid 0 MHz, as well as a more refined mesh | 69 |
| 6.12 | Vector plot of RWG basis function from [30] | 70 |
| 6.13 | Planar mesh of a ribbon dipole | 71 |
| 6.14 | Planar mesh with assigned triangle numbers | 72 |
| 6.15 | Portion of real “.out” file from FEKO describing triangles | 72 |
| 6.16 | Planar mesh edge being identified | 73 |
| 6.17 | Portion of real “.out” file from FEKO describing edges between triangles | 74 |
| 6.18 | Simulated model in FEKO for ribbon dipole, separated into 12 triangles with 11 edges between them | 75 |
| 6.19 | Setup of simulation done for FEKO extracted ribbon dipole impedance matrix with load and feed at center | 76 |
| 6.20 | Triangle and edge numbers in meshing identified from FEKO “.out” file | 76 |
| 6.21 | Results of the current spectrum on the central load from the Landt Integral Method and Conversion Matrices Method using a FEKO extracted impedance matrix of a ribbon dipole | 76 |
| 6.22 | Setup of simulation done for FEKO extracted ribbon dipole impedance matrix with load and feed at edge 10, away from the center | 77 |
| 6.23 | Results of the current spectrum on the off-center load from the Landt Integral Method and Conversion Matrices Method using the FEKO extracted impedance matrix of a ribbon dipole | 78 |
| 6.24 | Setup of the simulation in FEKO for the extracted ribbon dipole impedance matrix with load at edge 10 and feed at the center | 78 |

| | | |
|------|---|----|
| 6.25 | Results of the current spectrum for the off-center load and center feed for the Landt Integral Method and Conversion Matrices Method using the FEKO extracted impedance matrix of a ribbon dipole | 79 |
| 6.26 | Setup of the simulation done in FEKO for the extracted ribbon dipole impedance matrix with multiple loads | 79 |
| 6.27 | Results of the current spectrum in the center of two loads from the Landt Integral Method and Conversion Matrices Method using the FEKO extracted impedance matrix of a ribbon dipole | 79 |
| 6.28 | Result of the current spectrum on a planar antenna with a higher f_s to avoid 0 MHz, as well as a more refined mesh | 80 |

Abstract

Within traditional antenna design, the behavior of the antenna can be dictated by its physical dimensions and their proportions to a wavelength. Traditional electrically small antennas in particular face many limitations on factors such as their gain, quality factor, or bandwidth. The limitations on traditional antennas are based on the assumption that the antenna in question is a Linear Time-Invariant (LTI) component. This project proposes the introduction of time-varying loads to antennas in order to fundamentally alter the limitations assumed by electrical size. Non-LTI antennas however cannot be modeled and characterized by many traditional electromagnetic solvers used commonly. In this thesis, an expanded and generalized frequency domain method for analyzing time-varying loads on antennas is introduced. It combines traditional method of moments techniques with conversion matrices commonly used for time-varying circuit analysis. The Conversion Matrices Method (CMM) has shown to be promising, providing agreement with results found using a known time-domain method. This thesis provides the fundamental first step toward non-LTI antennas with an accurate method of modeling antennas with time-varying components.

Chapter 1

Introduction

Antenna size limitations, due to form-factor constraints, has driven many areas of research in traditional antenna design. While size is generally thought of as a physical dimension, for antennas, the implication of the size is based off its relation to the wavelength of the operating signal, known as the electrical size. For many antenna applications, an electrical size of a half-wavelength is simply too large to implement, especially for lower frequencies. Simply decreasing the electrical size is not always the solution, as it fundamentally changes the behavior of the antenna. Antennas with a physical size that is proportionally small enough to the wavelength to constitute such behavior limitations are called electrically small. Electrically small antennas are defined in [1] as any antenna whose maximum dimension is less than $\frac{1}{2\pi\lambda}$ represented in Figure 1.1. The constraints that electrical size present have been well documented in papers such as [1], [2], where conclusions on the antenna's efficiency and bandwidth can be drawn. This is backed up in [3]–[5], where an investigation into the quality factor (Q-factor) shows its reliance on the effective volume an antenna encompasses. They show that electrical size can place a limitation on the quality factor of an antenna, creating an inversely proportional relation to the bandwidth and antenna efficiency.

Electrical size, however, is not tied indefinitely to the physical dimensions of

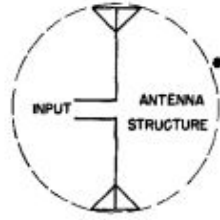


Figure 1.1: Omni-direction antenna used to prove limitations of electrically small antennas from [2]

the antenna. In many cases, in order to combat size restrictions for possibly lower frequencies, many techniques have been used to work around the electrical size dilemma. Capacitive or inductive loads can be placed along the antenna to provide a shift in the effective length of the antenna. While loading an antenna to increase its effective length seems like the obvious solution to the dilemma of physical size restriction, such loads do not change the instantaneous bandwidth and therefore the Q factor of the antenna. Despite the shift of the resonant frequency such typical loads can provide, the impedance bandwidth is still directly proportional to the electrical size. This can be present challenges in applications where a wider bandwidth is needed for system performance, but the required form factor makes the antenna electrically small.

Such limitations rely on the assumption that the antenna of interest is of traditional design. Traditional antennas are considered to be both passive and Linear Time-Invariant (LTI) components. By breaking those fundamental assumptions, a new avenue to bend the limitations of antenna design can be explored. This project explores the introduction of a linear time-varying load to an antenna shown in Figure 1.2 in order to bypass such limitations. It aims to give further insight into the behavior of such antennas, in particular their interaction with incident waves. This thesis will ideally give insight and intuition to the process of designing these anten-

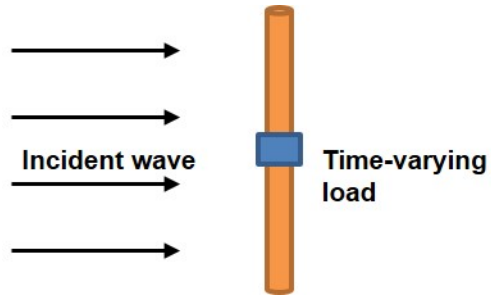


Figure 1.2: Visualization of proposed application of time-varying loads to antennas.

This project is not the first to utilize the effects of time-modulated loads to bend the rules of electrical size restriction on performance. While it has been shown in [6]–[8] that an electrically small antenna loaded with an active component can display higher performance, time-varying active loads are less deeply researched. In [9], the authors describe the design of a parametric slot antenna that is loaded with a varactor across the slot. The antenna is fed by a waveguide that couples both the input signal and pumping signal. While the most obvious difference between this antenna and the intentions of this project is its design as a transmit antenna rather than a receive. The paper also lacks methods to analyze the antenna and its behavior. [10] provides an example of a time-varying matching network with Direct Antenna Modulation (DAM) shown in Figure 1.3 implemented on a transmit antenna. The switching used to create the DAM effect was however not located on the antenna but rather before as a part of the feed. DAM does however show good evidence that such modulation is capable of achieving a broader band signal transmission than traditionally possible from an electrically small antenna.

The benefits of time-modulated loads have been explored in areas outside of antenna design for a variety of reasons, one of which being nonreciprocity. The authors in [11] used what was coined as Distributedly Modulated Capacitors, or

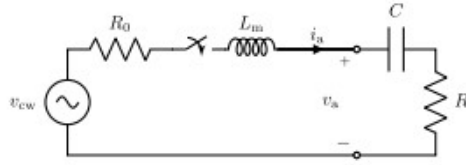


Figure 1.3: Example of direct antenna modulation created by a switch from [10]

DMCs, to create a nonreciprocal effect on a transmission line. By utilizing the frequency conversion that is often observed with the addition of time-varying components to a circuit, the transmit and receive signal on the transmission line can be separated into different frequency bands. This was suggested as an alternative to bulky ferrite material typically used in circulators. [12] utilizes the same concept of time-modulated resonators to create nonreciprocal bandpass filters. Analysis for this was done using what is called the spectral network parameters. This modification to traditional network parameters allow for the ability to apply them to Linear Time-Varying or LTV circuits. Many of the effects seen by time-varying loads are a result of the concept known as parametric amplification. Parametric amplification is defined in [13] as the application of a nonlinear or time-varying reactance through a pumping signal in order to achieve both amplification and frequency mixing.

The first challenge in the design of antennas that utilize time-modulated loads is the methods of which to model them. Due to the time-varying nature of this antenna modulation technique, traditional LTI antenna modeling techniques no longer apply. Many alternative modeling methods have been created to observe nonlinear loads in the time domain. These include those such as [14], [15] which utilize the finite difference time domain method (FDTD) to model the loaded antenna, while [16] uses the time-domain integral equation. While many methods have been developed to model the behavior of nonlinear loads, analysis for time-modulated loads has been more often been observed as a byproduct or extension of the original method. This

is most prevalent in the analytical methods that are solved using a time-stepping model such as that seen from Landt in [17]–[19]. This method takes the thin wire approximations described in [20], and performs a time-stepping operation to model the current distribution and spectrum on the antenna. Landt provides examples of this method operating for not only nonlinear loads, but time-modulated loads as well. Drawbacks to this method however circle around its time intensive nature.

A typical workaround to the drawbacks of time domain solutions is to move to the frequency domain. However, as established before, traditional frequency domain analysis techniques are not valid in a non-LTI system. Time-modulated loads have been modeled previously in the frequency domain in examples like [12] mentioned earlier with the spectral network parameters. The Reflection Algorithm, developed in [21] for microwave diode mixers, uses the known impedance behavior of the pumped load, as well as incident and reflected waves approaching the diode, in an iterative process to achieve a steady state solution. Huang [22] provided a method to analyze a wire antenna with a time-varying resistance by utilizing Method of Moments (MoM) to extract the impedance matrix of the antenna and conversion matrices from [23]. [24] did the same, but extended the implementation to time-varying capacitances as well. Both [22], [24] characterize the antenna being loaded with a single input impedance value in an equivalent circuit shown in Figure 1.4. This creates drawbacks to the method, as they do not provide a way to analyze the current at points on the antenna other than the load location. They also do not allow the application of multiple time-varying loads. These drawbacks are the motivation behind the developed and generalized technique introduced in this thesis.

This thesis will cover an expansion of the methods introduced by [22], [24]. The basis of those methods are combined with traditional antenna analysis from [20] to

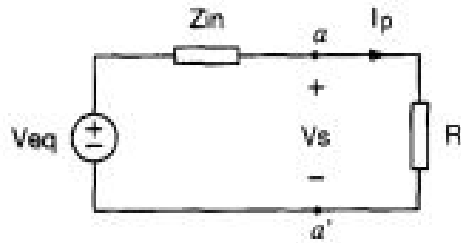


Figure 1.4: Equivalent circuit of antenna with modulated load from [22]

allow for a wider range of generalized use. The method developed is believed to be a useful stepping stone in the process of developing time-varying antennas for the applications mentioned before. This thesis will be structured into 7 chapters. Chapter 1 will act as the introduction, covering the motivation of the project and past work done in the field of time-varying loads on antennas. Chapter 2 will introduce the basics of method of moments and their applications. Chapter 3 will cover the Landt Integral Method, the time-domain analysis method used as the basis for comparison of the new developed method. Conversion matrices will be introduced in Chapter 4, and their application to antennas as well as the new expanded Conversion Matrices Method will be covered in Chapter 5. Chapter 6 will cover the techniques of Chapter 5 applied to impedance matrices extracted from FEKO. Finally, Chapter 7 will provide conclusions for the project, as well as a discussion on future work to be done in the research.

Chapter 2

Method of Moments

Much of the analysis techniques for this project are dependent on the antenna characteristics extracted by method of moments. Method of moments, or MoM, is defined by [25] as a technique that takes integral equations, and converts them into a linear system. In terms of electromagnetic computation, MoM takes the continuous integral equations that describe the electromagnetic behavior of an antenna, and uses them to compute the linear relation of charge distribution on the antenna from either a direct feed or incident wave. This is done by separating the antenna into discrete segments, and therefore finding the linear equations that describe the behavior on each of said segments. These linear equations are then described as matrix relations to solve for unknowns. This concept was first demonstrated on antennas by Harrington in [20], where its application to a variety electromagnetic computational problems was shown.

As stated, method of moments is a process that takes integral equations and creates a linear system of those equations by discretizing them. In order to understand this concept and apply it to more complicated problems, it is important to generalize the method itself. In order to describe this generalization, Harrington begins with the relation

$$L(f) = g, \tag{2.1}$$

where L is the linear operator, g is the forcing function like an excitation, and f is the unknown function like charge or current. This unknown function f is then discretized by N number of weighted basis functions

$$f = \sum_{m=-M}^M a_m f_m, \quad (2.2)$$

where $M = (N - 1)/2$ and a_m are the weighting coefficients. The weighted function can then be substituted into (2.1) resulting in the final equation

$$\sum_{m=-M}^M a_m L(f_m) \approx g. \quad (2.3)$$

This shows that the unknown current or charge can be described as a discrete sum of weighted values. In order to begin the process of using method of moments to perform electromagnetic computations on an antenna, the first step is to identify the boundary conditions that simplify the integral equation to be discretized. This chapter will begin with an overview of the boundary conditions of special cases made to obtain the needed integral equation to be solved, moving on to basis functions used to discretize said equation. Finally, methods presented by Harrington to analyze antennas using the linear matrix relations found using method of moments will be covered.

2.1 Thin Wire Antenna Approximation

The basis of method of moments is taking an integral equation, and converting it into a system of linear relations that can be enforced by certain boundary conditions. The specified integral equation and the boundary conditions that simplify it become increasingly important for solutions between the different type of antenna

geometries. This section will cover one of the most fundamental special cases, the thin wire antenna. As many of the beginning cases in this thesis feature a dipole antenna, it was thought of as important to give adequate explanation on the assumptions made on dipoles when using method of moments to analyze the antenna. In other cases, the general integral form of Maxwell's equations can be applied.

While the standard integral Maxwell's equations can be applied to any geometry, these equations can be simplified down when certain assumptions can be made about the structure. The derivation of the thin wire antenna approximation integral equations is covered in great detail in [20], [25], [26]. This derivation begins with a thin wire aligned with the z-axis shown in Figure 2.1 and Green's function

$$G(\rho, z - z') = \frac{e^{-jkR}}{R}, \quad (2.4)$$

where k is the propagation constant of the material and $R = \sqrt{(z - z')^2 + \rho^2}$. This Green's Function is an approximation of the full form version, and is applicable to a thin wire antenna. The function can then be integrated over the surface area of the conductor in order to find the magnetic vector potential

$$A_z(\rho, \phi, z) = \frac{\mu}{4\pi} \int_{-l/2}^{l/2} \int_0^{2\pi} \frac{I_z(z') e^{2jkR}}{2\pi R} d\phi' dz' \quad (2.5)$$

where l is the length of the antenna and $I_z(z')$ is the current along the wire. This surface integral can now be simplified to a line integral by making two major assumptions about the structure. The first of which is that at either ends of the dipole the current is zero, and the second being that the radius is of a size much smaller in proportion to the length. These two assumptions make the impact of the $d\phi$ portion of the integral much more negligible, and reduces the thin wire approximation

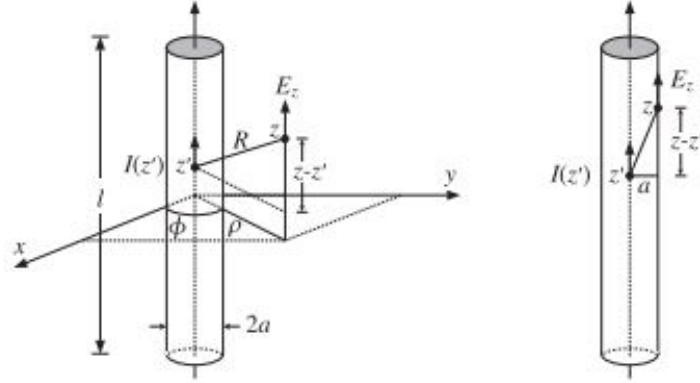


Figure 2.1: Model used for the thin wire antenna approximation from [26]

magnetic vector potential to the equation

$$A_z(\rho, z) = \frac{\mu}{4\pi} \int_{-l/2}^{l/2} I_z(z') \frac{e^{-jkR}}{R} dz' \quad (2.6)$$

2.1.1 Hallen and Pocklington Equations

The magnetic vector potential can then be used to determine the incident and radiated field acting upon the antenna. This calculation is only reliant however on a single assumption, that the total electric field is a summation of the incident and reflected fields and is equal to zero on the boundary of the wire, described by $E_{total} = E_{rad} + E_{inc} = 0$. This can be attributed to a PEC approximation of the wire, where an electric field cannot exist in a perfect electric conductor. The incident field can then be calculated by applying the magnetic vector potential of a thin wire antenna with the relation

$$E_{inc} = \frac{j}{\omega\mu\epsilon} \left[\frac{\delta^2}{\delta z^2} + k^2 \right] A_z \quad (2.7)$$

derived from Maxwell's equations. This relation can be expanded in two different ways, known as the Hallen and Pocklington integral equations. Hallen's Integral Equation is the direct result of inserting the magnetic vector potential into (2.7), stating

$$E_{inc} = \frac{j}{\omega\epsilon} \left[\frac{\delta^2}{\delta z^2} + k^2 \right] \int_{-l/2}^{l/2} I_z(z') \frac{e^{-jkR}}{4\pi R} dz'. \quad (2.8)$$

By transferring the differential operator to within the integral, one can derive Pocklington's Integral Equation as

$$E_{inc} = \frac{j}{\omega\epsilon} \int_{-l/2}^{l/2} I_z(z') \left[\frac{\delta^2}{\delta z^2} + k^2 \right] \frac{e^{-jkR}}{4\pi R} dz'. \quad (2.9)$$

Both Pocklington's and Hallen's equations have their own particular costs and benefits. Hallen, while providing a more accurate calculation that converges much faster, is a more complicated calculation. Pocklington's equation is easier to compute, but requires the antenna be analyzed at a higher number of segments to reach the same accuracy as Hallen. This relationship can be observed in Figure 2.2.

2.2 Basis Functions

The weighted basis function that dictates the discretization described before is of utmost importance. It can have great influence on the accuracy of the solution. The utilization of basis functions that match the weighted functions to solve method of moments problems is called Galerkin's Method [25]. This section will cover a few examples of common basis functions used specifically for thin wire antennas.

The delta basis function is one of the simplest and most intuitive ways to approach a weighted basis function for the Galerkin Method. It follows a very similar protocol to the method of point matching, evaluating at specified discrete points on

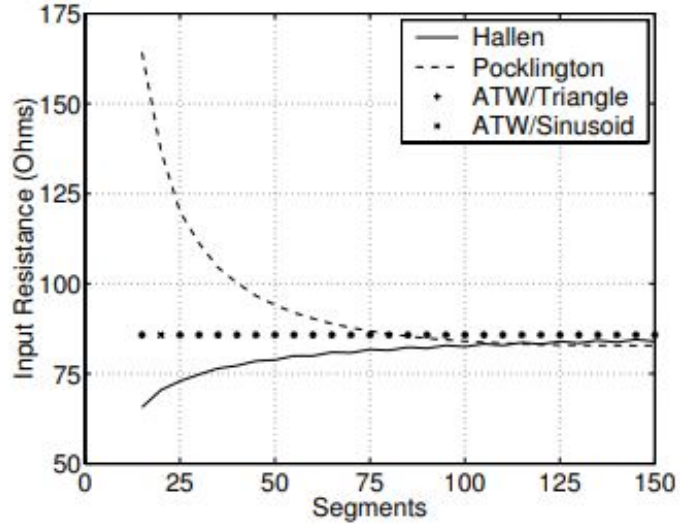


Figure 2.2: Accuracy of Hallen vs. Pocklington integral equations from [25]

the antenna. While the results are similar to simple point matching, using the delta basis function with the Galerkin Method is achieved by utilizing the basis function

$$B(z) = \delta(z)\Delta, \quad (2.10)$$

where δ is the width of the narrow pulses, and $\Delta = L/N$ is the spacing between those pulses. A visualisation of the delta basis function is provided in Figure 2.3. It can be viewed rather as a direct sampling at the center of the segment.

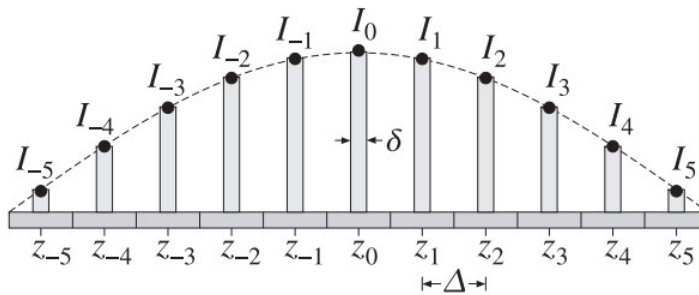


Figure 2.3: Representation of delta basis function from [26]

The pulse basis function is an extension of the delta basis function. Rather than a single sampling at the center of the segment, the pulse basis function looks at the evaluation of the current or charge on the antenna as a step function over the entirety of the segment. The resulting equation for the basis function is

$$B(z) = \begin{cases} 1 & \text{if } |z' - z_m| \leq \frac{1}{2}\Delta, \\ 0, & \text{otherwise} \end{cases}, \quad (2.11)$$

where Δ is the same as the delta basis function and $|z' - z_m|$ is the location centered on the m^{th} segment. Each value at that central point is assigned to the whole segment, providing continuity. The pulse basis function is shown in Figure 2.4.

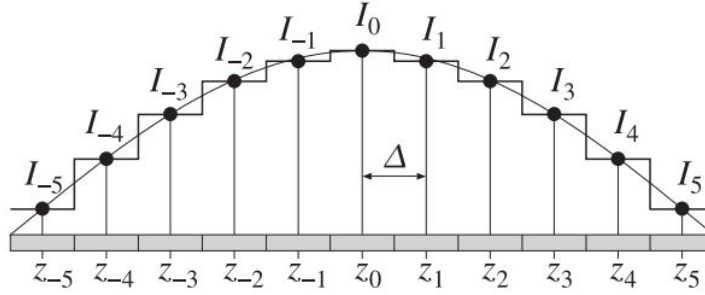


Figure 2.4: Representation of pulse basis function from [26]

The triangular basis function varies from the prior two, as instead of assessing the behavior of a single segment, it identifies the interaction between two segments. The values of the basis function are then assigned to the edges between segments rather than the center of the segments. This results in a $N = 11$ case actually made up of 10 segments with 11 edges. The triangular basis function [26] is defined by

the equation

$$B(z) = \begin{cases} 1 - \frac{|z|}{\Delta} & \text{if } |z| \leq \Delta \\ 0, & \text{otherwise} \end{cases} \quad (2.12)$$

where the width of each segment is $\Delta = L/(N - 1)$, differing from the pulse and delta basis functions.

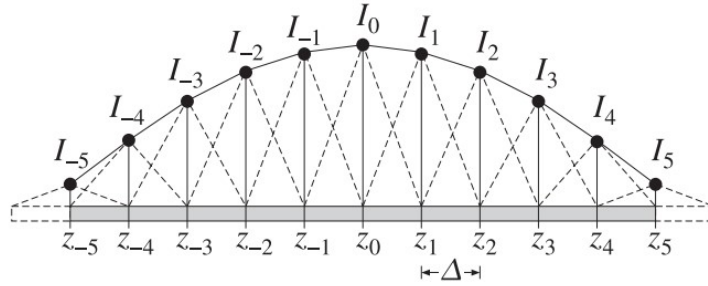


Figure 2.5: Representation of piecewise triangular basis function from [26]

The final basis function to be discussed is the Numerical Electromagnetics Code (NEC) sinusoidal basis function. The NEC is a public-domain program widely available for modeling antennas. It utilizes Pocklington's integral equation as well as a sinusoidal basis in order to complete its computation. The basis function used by the NEC is significantly more complicated than the basis functions discussed so far in this chapter.

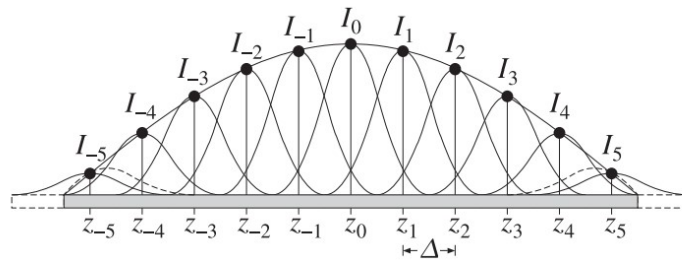


Figure 2.6: Representation of piecewise NEC basis function from [26]

For the Galerkin Method, the basis function can then be used to calculate the impedance matrix using the equation

$$Z_{nm} = \frac{j\eta}{2\pi} \int_{-L/2}^{L/2} \int_{-L/2}^{L/2} B(z - z_n)G(z - z')B(z' - z_m)dzdz' \quad (2.13)$$

where $G(z)$ is the kernel, serving as a linear map between the vector spaces of the voltage and the current. This equation samples that linear map based off of the basis equations to create the impedance matrix.

2.3 Antenna Analysis using Method of Moments

Once the impedance matrix has been extracted, analyzing the characteristics of various antenna geometries becomes a fairly simple linear matrix calculation. This is done in Harrington by describing the antenna as a multi-port system, with each of the sampled points denoted by the basis function as its own individual point. The relation

$$[v] = [z][i] \quad (2.14)$$

is used where $[v]$ and $[i]$ are the port voltages and currents respectively. The value of the impedance matrix can then be deduced using the relation

$$z_{ab} = \frac{v_a}{i_b} \quad (2.15)$$

where the ports are open-circuited. This approach allows for method of moment computations to be done where loads are applied, as well as a variety of different excitations. This section will cover the ways Harrington outlines utilizing such methods for extended antenna analysis.

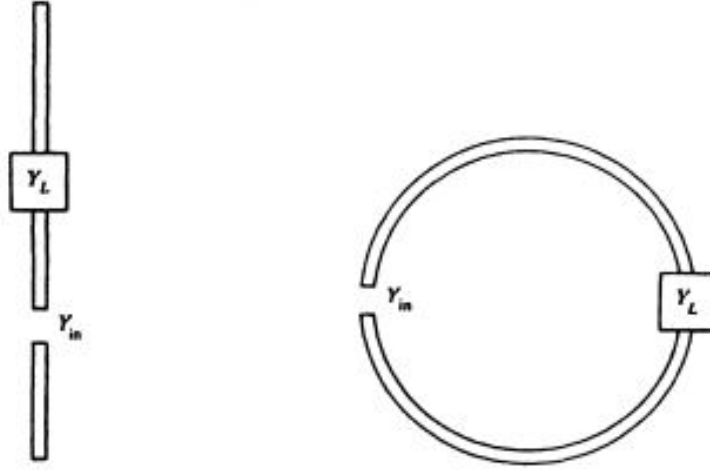


Figure 2.7: Figure representing antennas being loaded using multi-port system from [20]

2.3.1 Applying Loads

One extension Harrington describes is the ability to use the extracted method of moments impedance matrix, and manipulate it in order to understand the behavior of a load on the antenna. In order to describe the process of applying a load, Harrington describes the antenna with a single load as a two-port system. One port is the observation point along the antenna, and the secondary port is the load location itself shown in Figure 2.7. This two-port relation is as follows

$$\begin{bmatrix} i_1 \\ i_2 \end{bmatrix} = \begin{bmatrix} y_{11} & y_{12} \\ y_{21} & y_{22} \end{bmatrix} \begin{bmatrix} v_1 \\ v_2 \end{bmatrix}. \quad (2.16)$$

Due to reference conditions, the relation of the loaded admittance to its location is

$$i_2 = -Y_L v_2. \quad (2.17)$$

A physical representation of this relation is shown in Figure 2.7. If the two-port

admittance matrix and the antenna load is known, it can be solved to result in the following relation

$$Y_{in} = y_{11} - \frac{y_{12}y_{21}}{y_{22} + Y_L} \quad (2.18)$$

which shows the input admittance at the observation point with the load at point 2. The use of the two-port system is a very valuable approach to loading the antenna, but in order to move further to multiple loads along the antenna, the approach must be applied to the entire impedance matrix. To show the approach of loading using the full antenna, one first begins with the impedance matrix Z ,

$$Z = \begin{bmatrix} z_{11} & z_{12} & z_{13} & \dots & z_{1N} \\ z_{21} & z_{22} & z_{23} & \dots & z_{2N} \\ z_{31} & z_{32} & \ddots & & \vdots \\ \vdots & & & \ddots & \vdots \\ z_{N1} & \dots & \dots & \dots & Z_{NN} \end{bmatrix}. \quad (2.19)$$

Using the same reference conditions as the single load case, the load impedance is subtracted from the self-impedance at the location the load is placed. For example, a load placed on the second segment will result in an impedance matrix

$$Z - Z_L = \begin{bmatrix} z_{11} & z_{12} & z_{13} & \dots & z_{1N} \\ z_{21} & z_{22} - Z_L & z_{23} & \dots & z_{2N} \\ z_{31} & z_{32} & \ddots & & \vdots \\ \vdots & & & \ddots & \vdots \\ z_{N1} & \dots & \dots & \dots & Z_{NN} \end{bmatrix}. \quad (2.20)$$

This new loaded impedance matrix can now be used for method of moment solutions.

2.3.2 Excitations

This section will cover the three primary methods used to excite specifically linear thin wire antennas. These methods can be extended to different antenna geometries, but for the purpose of the applications outlined in this thesis, the focus remained on linear antennas. The three main methods that will be covered are the delta-gap model, the magnetic frill model, and the plane wave source. Models of the delta-gap model and plane wave source from [26] are shown in Figure 2.8.

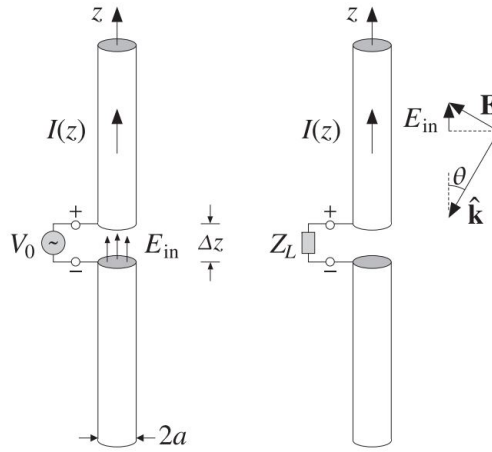


Figure 2.8: Excitation models of delta-gap and plane wave source from [26]

Two excitation models are typically used for transmit antennas as their application is concentrated on a single segment, the location of the feed. The first of which is the delta-gap model which assumes that an electric field is only applied to a specific gap, Δz . The resulting relationship from the experienced E-field and the induced voltage is

$$V_0 = E_{in}\Delta z, \quad (2.21)$$

where V_0 and E_{in} are the voltage and E-field on the specified gap, or in many cases, the segment being excited. It is important to note that $[V]$ and $[E]$ are related

through a factor called d , which is defined by

$$d = 2 * k * \Delta^2, \quad (2.22)$$

where k is the propagation constant of the medium, and Δ is the length of each segment. The relation of $[V]$ and $[E]$ is defined as

$$[V] = \begin{bmatrix} E_1 * d \\ E_2 * d \\ E_3 * d \\ \vdots \\ E_N * d \end{bmatrix}. \quad (2.23)$$

Therefore, an antenna excitation matrix that is excited centrally using the delta-gap model would result in the matrix

$$[V] = \begin{bmatrix} 0 \\ 0 \\ \vdots \\ E_{N/2} * d \\ \vdots \\ 0 \\ 0 \end{bmatrix}. \quad (2.24)$$

The second single segment excitation model is the magnetic frill model, shown in Figure 2.9. Instead of modeling the source as a current being induced by an incident E-field on the specified segment, the magnetic frill models the source as a magnetic field circling the conductor at a radius b that is inducing a current on the conductor

of radius a . The model is defined by the equation

$$E_{in}(z) = \frac{V_0}{2\ln(b/a)} \left[\frac{e^{-jkR_a}}{R_a} - \frac{e^{-jkR_b}}{R_b} \right] \quad (2.25)$$

where $R_a = \sqrt{z^2 + a^2}$ and $R_b = \sqrt{z^2 + b^2}$.

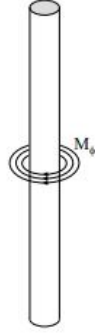


Figure 2.9: Excitation model of magnetic frill source from [25]

The final excitation model is the plane wave source, used primarily for receive antennas. Shown in Figure 2.8, the plane wave source assumes the incident wave is approaching the antenna at a specified angle θ , and that all segments in the method of moments solution are excited. The weighting at which each segment is specified is determined by the angle of incidence itself. The equation for the incident field is

$$E_{in}(z) = E_0 \sin\theta e^{jkz\cos\theta}. \quad (2.26)$$

The resulting matrix for an incident plane wave excitation will be

$$[V] = \begin{bmatrix} E_0 * d \sin\theta e^{jk\cos\theta} \\ E_0 * d \sin\theta e^{j2k\cos\theta} \\ E_0 * d \sin\theta e^{j3k\cos\theta} \\ \vdots \\ E_0 * d \sin\theta e^{jNk\cos\theta} \end{bmatrix}. \quad (2.27)$$

Due to the end result of this project being a receive antenna, the plane-wave model is most heavily used in the entirety of this document.

2.4 Summary

Method of moments is a fundamental theory for electromagnetic computation. It utilizes boundary conditions of specific geometries and weighted basis functions to create discretized linear relations of Maxwell's equations in integral form. Harrington has shown that it can be a useful tool in understanding the behavior of an antenna as it is loaded and fed with differing types of excitations. The following chapter will cover a time-domain method that utilizes method of moments to characterize time-varying and nonlinear loads on antennas.

Chapter 3

Landt Integral Method for Time-Varying Loads

With the implementation of a time-varying load, the use of a time domain solution appears to be the most intuitive approach. This section will cover the method described in [17]–[19] by Jeremy Landt. For the remainder of the chapters, the method outlined in this chapter will be referred to as the Landt Integral Method. As stated before, method of moments is the conversion of integral equations into a linear form. This principle is the basis for this time domain method for analyzing nonlinear and time-varying loads on antennas. The Landt Integral Method will be used as the basis for comparison of the new developed method.

3.1 Integral Equation Basis

While it may seem intuitive to simply take a finite difference time domain approach for the solution in the time domain, [15] states that for a structure as simple as a wire antenna, the computational time will be smaller with the application of method of moments. For applications outside of this project that utilize more complicated geometries, a finite difference time domain method may be required. In order to create the linear matrix relation, the integral equation applicable must first be identified.

The integral equation used by [17] was

$$\hat{s} \cdot \vec{E}^{inc}(\vec{r}, t) = \frac{\mu_0}{4\pi} \int_{C(\vec{r})} \left[\frac{\hat{s} \cdot \hat{s}'}{R} \frac{\delta}{\delta t'} I(s', t') + c \frac{\hat{s} \cdot \vec{R}}{R^2} \cdot \frac{\delta}{\delta s} I(s', t) - c^2 \frac{\hat{s} \cdot \vec{R}}{R^3} q(s', t') \right] ds', \quad (3.1)$$

where $\vec{E}^{inc}(\vec{r}, t)$ is the incident E-field at observation point \vec{r} and time t . \hat{s} and \hat{s}' are unit vectors parallel to $C(\vec{r})$ at \vec{r} and \vec{r}' . $I(s', t')$ and $q(s', t')$ are the current and charge at point s' and time t' . c and μ_0 are the speed of light and permeability of free space respectively. This integral equation can then be reduced to the linear matrix relation of

$$[E_v^I] + [E_v^S] = [Z][I_v] \quad (3.2)$$

where $[E_v^I]$ is the incident E-field at time step v , $[E_v^S]$ is the scattered E-field at time step v , and $[I_v]$ is the current on the antenna at time step v .

3.2 Loaded Matrix Relations

The linear matrix relation found in the previous section does not account for the application of a load. In order to do so, the relation must be slightly altered in order to derive the computations done by Landt. This altered relation is

$$[E_v^I] + [E_v^S] = [Z][I_v] + [Z_L][I_v], \quad (3.3)$$

where $[I_v]$ is the unknown current of the loaded antenna at time step v and $[Z_L]$ is an impedance matrix for the added load. In order to derive the matrix relations that dictate Landt's Integral Method, the antenna and its load is first observed as a

two-port system. This makes the impedance matrix a 2×2 matrix

$$[Z] = \begin{bmatrix} Z_{11} & Z_{12} \\ Z_{21} & Z_{22} \end{bmatrix} \quad (3.4)$$

where Z_{11} and Z_{22} are the self impedances of the load location and observation point, respectively. Z_{12} and Z_{21} are the impedances between the two locations on the antenna. The 2×2 matrix representing the load value is

$$[Z_L] = \begin{bmatrix} Z_L & 0 \\ 0 & 0 \end{bmatrix} \quad (3.5)$$

where it can be seen that the load is only located at the same place on the antenna as the self impedance Z_{11} . If the load is time-varying, the value of Z_L is also changing with each time step v . In order to stay consistent with [20], the same assumptions are made on reference conditions, and the following constraint

$$E_{1v} = -[Z_L]I_{1v} \quad (3.6)$$

is applied, where E_{1v} and I_{1v} are the E-field and current at the location of the load at time step v . The expansion of (3.3) for the two-port system is then

$$\begin{bmatrix} E_{1v} \\ E_{2v} \end{bmatrix} = \left(\begin{bmatrix} Z_{11} & Z_{12} \\ Z_{21} & Z_{22} \end{bmatrix} - \begin{bmatrix} Z_L & 0 \\ 0 & 0 \end{bmatrix} \right) \begin{bmatrix} I_{1v} \\ I_{2v} \end{bmatrix}. \quad (3.7)$$

The relation

$$[E_v] = [Z][I_v^u] \quad (3.8)$$

can then be substituted into the expansion, where $[I_v^u]$ is the current on the unloaded antenna resulting in

$$\begin{bmatrix} I_{1v}^u \\ I_{2v}^u \end{bmatrix} = \left(\begin{bmatrix} 1 & 0 \\ 0 & 1 \end{bmatrix} + \begin{bmatrix} Z_{11} & Z_{12} \\ Z_{21} & Z_{22} \end{bmatrix}^{-1} \begin{bmatrix} -Z_L & 0 \\ 0 & 0 \end{bmatrix} \right) \begin{bmatrix} I_{1v} \\ I_{2v} \end{bmatrix}. \quad (3.9)$$

To now solve for the unknown current accounting for the load, the final equation is

$$\begin{bmatrix} I_{1v} \\ I_{2v} \end{bmatrix} = \left(\begin{bmatrix} 1 & 0 \\ 0 & 1 \end{bmatrix} + \begin{bmatrix} Z_{11} & Z_{12} \\ Z_{21} & Z_{22} \end{bmatrix}^{-1} \begin{bmatrix} -Z_L & 0 \\ 0 & 0 \end{bmatrix} \right)^{-1} \begin{bmatrix} I_{1v}^u \\ I_{2v}^u \end{bmatrix}. \quad (3.10)$$

This equation is then evaluated for all values of time step v , and combined to complete the waveform for the current distribution on the antenna.

The matrix relation for a two port can then be expanded to a full method of moments impedance matrix for an antenna. An example of this can be seen in Figure 3.1 where a dipole separated into three segments is loaded with a time-varying resistance R . The resulting calculation of the current on the antenna with the time-varying load at a single time step will be

$$\begin{bmatrix} I_{1v} \\ I_{2v} \\ I_{3v} \end{bmatrix} = \left(\begin{bmatrix} 1 & 0 & 0 \\ 0 & 1 & 0 \\ 0 & 0 & 1 \end{bmatrix} + \left(\begin{bmatrix} Z_{11} & Z_{12} & Z_{13} \\ Z_{21} & Z_{22} & Z_{23} \\ Z_{31} & Z_{32} & Z_{33} \end{bmatrix}^{-1} \begin{bmatrix} 0 & 0 & 0 \\ 0 & -R_v & 0 \\ 0 & 0 & 0 \end{bmatrix} \right) \right)^{-1} \begin{bmatrix} I_{1v}^u \\ I_{2v}^u \\ I_{3v}^u \end{bmatrix}, \quad (3.11)$$

where R_v is the value of the time-varying resistance R at time step v . Once again, this is evaluated at each time step, and compiled to find the total current over the whole time sample.



Figure 3.1: Example of wire antenna with a time-varying Load

3.3 Results and Applications

In order to show the results of this method, as well as prove the validity of the replication done in MATLAB, an example problem from [17] will be used. The example presented is a 9 m dipole that has a radius of 0.2 m. It is divided into 9 segments and experiences a 16 MHz incident E-field wave of 1 V/m. It is centrally loaded with a time-varying resistance oscillating at the rate

$$R(t) = 500(1 + \sin(\omega_p t)) \Omega \quad (3.12)$$

where $\omega_p = 2\pi(4 \text{ MHz})$. It is important to note that in [17], Landt only provides results as the relative magnitude of the E-field spectrum on the load, but does not specify at what distance the magnitude is being evaluated. Due to this, the current spectrum of the computed results will be compared to Landt's as this is known to be proportional.

The results of the specified example provided by [17] are shown in Figure 3.2 along with the results of the MATLAB code replicating Landt's process. The results show great agreement between the two for the same example, particularly in the

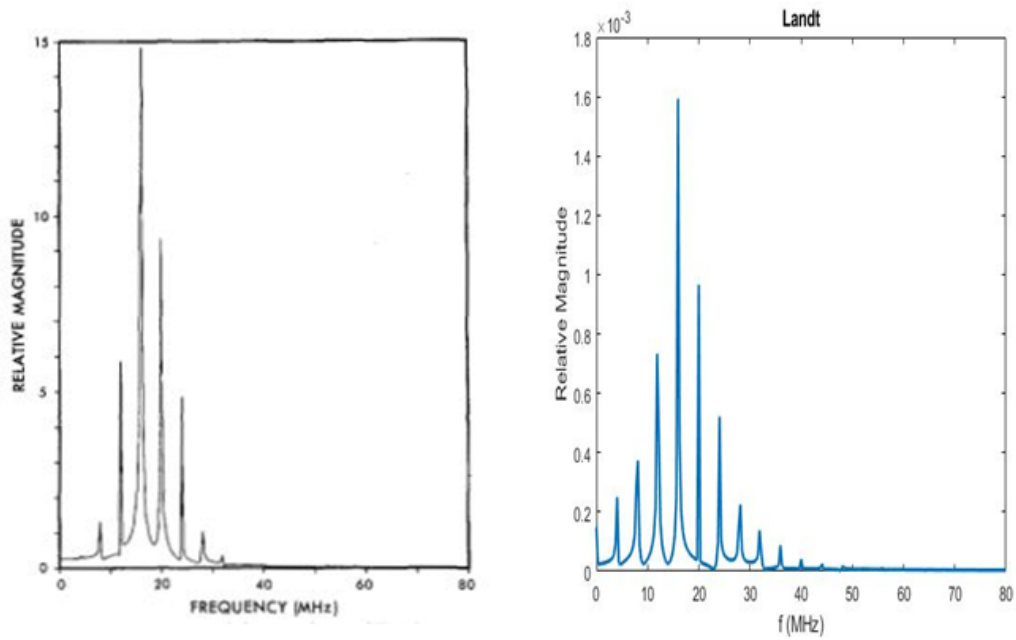


Figure 3.2: Results of E-field spectrum from [17] of provided example along with results of current spectrum from MATLAB code meant to replicate Landt example

spectrum shape between the two. Both results show spectral spreading when the addition of a time-varying load is made on an antenna. The replicated MATLAB code is also capable of recreating the current waveform from [17]. Figure 3.3 shows the waveform of the E-field from [17] and the current waveform from the replicated MATLAB code. The results are shown to be proportional to the results provided by Landt as expected.

3.4 Summary

This chapter covered a time-domain method for analyzing time-varying and non-linear loads on antennas called the Landt Integral Method. While this method was written to be performed in FORTRAN, a replication was produced for the purposes of this project in MATLAB. It is believed that this method will provide a

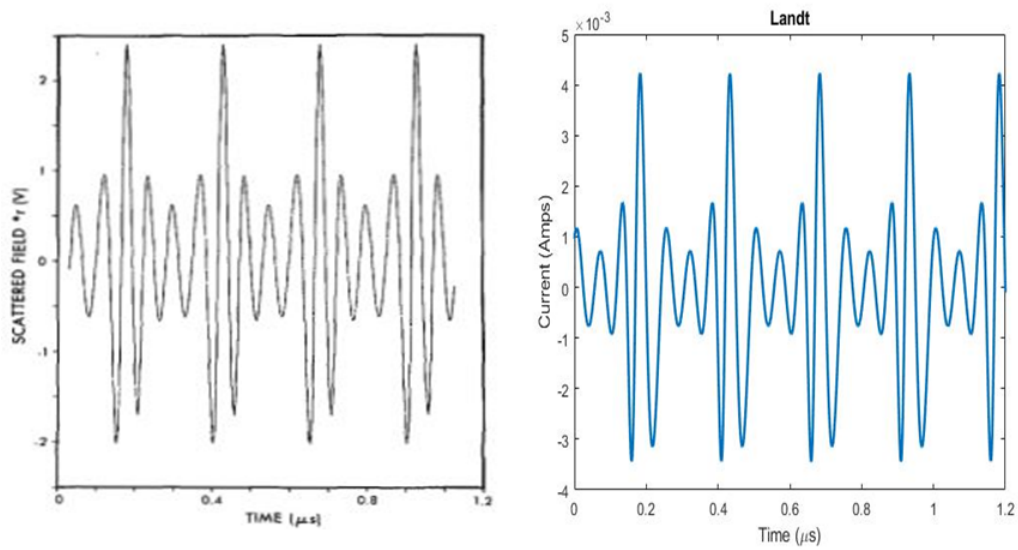


Figure 3.3: Waveform of field vs. time from [17] and the result of current vs. time -from MATLAB code meant to replicate the example

standard for the performance of other methods throughout the continuation of this project. The next chapter will introduce methods used for time-varying elements in the frequency domain; however, later chapters will once again call back to the Landt Integral Method for validation.

Chapter 4

Introduction of Conversion Matrices

In basic circuit analysis, the introduction of analysis in the frequency domain allows for increased ease and speed of computation. The frequency domain is most commonly used for its ability to simplify mathematical relations from differential equations into algebraic relations. Conversion matrices are introduced by Stephen Maas in [23], [27] as a way to model a time-varying load and perform basic circuit analysis in the frequency domain. This chapter will outline the background, formulation, and application of such matrices.

4.1 Background of Large-Signal/Small-Signal Analysis

Large-Signal/Small-Signal analysis is introduced in [23] as a means to analyze the effects of a small signal on a device that is “pumped” by a larger signal. Typically the device is nonlinear and often a mixer. The harmonic-balance method is first used to perform the large-signal analysis, producing a linear time-varying or LTV equation that can be used to represent the non-linearity in the device. Conversion matrices are used in the small-signal analysis portion of large-signal/small-signal analysis. They provide a way to model LTV elements, and perform circuit analysis of both LTV and static components. For this project, the former portion of large-

$$\begin{bmatrix} V_{-N}^* \\ V_{-N+1}^* \\ V_{-N+2}^* \\ \dots \\ \dots \\ V_{-1}^* \\ V_0 \\ V_1 \\ \dots \\ \dots \\ V_N \end{bmatrix} = \begin{bmatrix} R_0 & R_{-1} & R_{-2} & \dots & R_{-2N} \\ R_1 & R_0 & R_{-1} & \dots & R_{-2N+1} \\ R_2 & R_1 & R_0 & \dots & R_{-2N+2} \\ \dots & \dots & \dots & \dots & \dots \\ \dots & \dots & \dots & \dots & \dots \\ R_{N-1} & R_{N-2} & R_{N-3} & \dots & R_{-N-1} \\ R_N & R_{N-1} & R_{N-2} & \dots & R_{-N} \\ R_{N+1} & R_N & R_{N-1} & \dots & R_{-N+1} \\ \dots & \dots & \dots & \dots & \dots \\ \dots & \dots & \dots & \dots & \dots \\ R_{2N} & R_{2N-1} & R_{2N-2} & \dots & R_0 \end{bmatrix} \begin{bmatrix} I_{-N}^* \\ I_{-N+1}^* \\ I_{-N+2}^* \\ \dots \\ \dots \\ I_{-1}^* \\ I_0 \\ I_1 \\ \dots \\ \dots \\ I_N \end{bmatrix}$$

Figure 4.1: Format of time-varying component conversion matrix along with excitation matrices from [23]

signal/small-signal analysis is not needed as all components, the antenna and its loads, are LTV by choice. Therefore, this chapter will only focus on small-signal analysis done with conversion matrices.

4.2 Structure of Conversion Matrices

Conversion matrices are simply the frequency domain relation of the voltages and currents of time-varying circuits. In order to use them to perform circuit analysis, the formation of the matrices is key. The structure of the matrix varies however between time-varying components, static components, and the sources in the circuit. This section will detail the methodology of formatting conversion matrices based off the type of component.

4.2.1 Excitations

The format for excitations to be used in tandem with conversion matrices of components is very simple. In order to create the voltage and current matrices that can accurately display the mixing properties of time-varying loads, they must be formatted a certain way. Both the voltage and current matrices are made from the frequency notation

$$v'(t) = \sum_{n=-\infty}^{\infty} V_n e^{jn\omega_n t} \quad (4.1)$$

and

$$i'(t) = \sum_{n=-\infty}^{\infty} I_n e^{jn\omega_n t} \quad (4.2)$$

where ω_n is the mixing frequency. The mixing frequency is defined by

$$\omega_n = \omega_s + n\omega_p, \quad (4.3)$$

where ω_s is the signal frequency, and ω_p is the frequency at which the load is oscillating. A visualization of the mixing frequencies is shown in Figure 4.2. The format of the excitation matrices can be seen in Figure 4.1, where the subscript denotes the value of n when calculating ω_n . It is important to note that this is in fact not the Fourier series of the voltage and current as the element values are evaluated at each mixing frequency rather than at each harmonic.

4.2.2 Static Components

While static components have impedance values that do not change with time, components such as the impedance of an antenna segment can still change with frequency. Therefore it is still important to put the impedance in a form that still de-

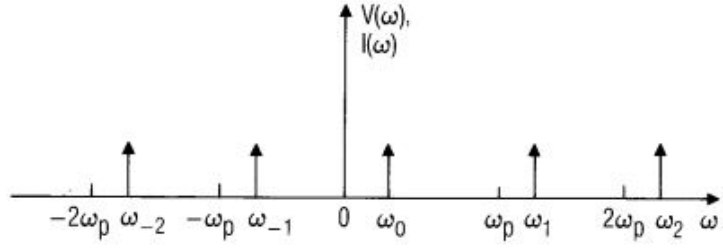


Figure 4.2: Mixing frequency representation from [23]

describes the behavior of the component over the mixing frequencies being evaluated. The format of static component conversion matrices is very similar to that of the excitations. Rather than a Fourier series, each element is determined by its value at the specified mixing frequency ω_n similar to the excitations. The signal frequency, or mixing frequency evaluated at $n = 0$ where $\omega_0 = \omega_s + 0(\omega_p)$ is placed at the center of the matrix. The positive mixing frequencies are placed further along the diagonal, and their negative mixing frequency counterparts are placed before the signal frequency. The values of the component at each of the different mixing frequencies in the diagonal matrix is shown in Figure 4.3.

$$\mathbf{Z} = \begin{bmatrix} Z^*(-\omega_N) & 0 & \dots & 0 & 0 & 0 & \dots & 0 \\ 0 & Z^*(-\omega_{N+1}) & \dots & 0 & 0 & 0 & \dots & 0 \\ \dots & \dots & \dots & \dots & \dots & \dots & \dots & \dots \\ 0 & 0 & \dots & Z^*(-\omega_{-1}) & 0 & 0 & \dots & 0 \\ 0 & 0 & \dots & 0 & Z^*(\omega_0) & 0 & \dots & 0 \\ 0 & 0 & \dots & 0 & 0 & Z(-\omega_1) & \dots & 0 \\ \dots & \dots & \dots & \dots & \dots & \dots & \dots & \dots \\ 0 & 0 & \dots & 0 & 0 & 0 & \dots & Z(\omega_N) \end{bmatrix}$$

Figure 4.3: Format of static impedance conversion matrix from [23]

4.2.3 Time-Varying Components

Linear time-varying components are the primary reason of the existence and need of conversion matrices. It is then understandable why the formulation of them is of utmost importance. The basis of the conversion matrix for a time-varying component is the Fourier series of the time-varying equation that describes the load. The Fourier series is a function that describes a period function as a summation of a sinusoid and its harmonics. Specifically for conversion matrices, the complex Fourier coefficients must be extracted from the series in order to find the element values for the conversion matrix.

For a time-varying resistive load oscillating at a rate of ω_p , the relation between the resistance over time and its Fourier coefficients is described by the equation

$$R(t) = \sum_{n=-\infty}^{\infty} R_n e^{jn\omega_p t}, \quad (4.4)$$

where the values for R_n are the complex Fourier coefficients for each of the harmonics. In order to calculate the values for R_n , the coefficients can be calculated using the equations[28]

$$a_n = \frac{2}{T} \int_0^T R(t) * \cos(2\pi f_p n t) \quad (4.5)$$

and

$$b_n = \frac{2}{T} \int_0^T R(t) * \sin(2\pi f_p n t), \quad (4.6)$$

where $T = \frac{1}{f_p}$ is the period of the signal. These coefficients can then be converted into the complex form

$$R_n = \frac{a_n + jb_n}{2}. \quad (4.7)$$

It however is not possible to implement an infinite conversion matrix, therefore these coefficients are evaluated for a number of harmonics N , both positive and negative, from $n = -2N$ to $2N$. Once the complex coefficients are evaluated for all of the values of n , they are placed into the conversion matrix format shown in Figure 4.1. Note that value of the element R_{-N} is the complex conjugate of R_N .

In order to show an example of a resistive conversion matrix, a time-varying resistance of value

$$R(t) = 500 * (1 + \sin(2\pi(4 \text{ MHz})t))\Omega \quad (4.8)$$

is used. To keep the example as simplified as possible, only one harmonic was evaluated meaning $N = 1$. The complex Fourier series for this load evaluate to be

$$R(t) = 500 + (-3.38 \times 10^{-12} + i2.5 \times 10^2)e^{j(4\text{MHz})t} + (-5.93 \times 10^{-14} + i3.77 \times 10^{-14})e^{j(8\text{MHz})t}\Omega. \quad (4.9)$$

These values can then be inserted into the resistive conversion matrix, with the complex conjugate being taken of the negative frequency values. The resulting conversion matrix \mathbf{R} is

$$\mathbf{R} = \begin{bmatrix} 500 & -3.38 \times 10^{-12} - i2.5 \times 10^2 & -5.93 \times 10^{-14} - i3.77 \times 10^{-14} \\ -3.38 \times 10^{-12} + i2.5 \times 10^2 & 500 & -3.38 \times 10^{-12} - i2.5 \times 10^2 \\ -5.93 \times 10^{-14} + i3.77 \times 10^{-14} & -3.38 \times 10^{-12} + i2.5 \times 10^2 & 500 \end{bmatrix} \Omega. \quad (4.10)$$

A time-varying capacitive or inductive load requires slightly different treatment. Such reactance conversion matrices require the multiplication of a frequency conversion matrix shown in Figure 4.4 when applied to circuit analysis. Figure 4.4

shows the format of the frequency matrix closely reflects that of the static component conversion matrix with the diagonal values being defined by the mixing frequencies. The reasoning behind this can be shown by the charge found in a time-varying capacitor

$$q'(t) = c(t)v(t), \quad (4.11)$$

which can be expanded in discrete form to

$$\sum_{k=-\infty}^{\infty} Q_k e^{j\omega_k t} = \sum_{n=-\infty}^{\infty} \sum_{m=-\infty}^{\infty} C_n V_m e^{j\omega_{m+n} t} \quad (4.12)$$

The relation of current to charge is defined as

$$i'(t) = \frac{d}{dt} q'(t), \quad (4.13)$$

and when put in discrete form with (4.12) substituted in for the charge has the form

$$\sum_{k=-\infty}^{\infty} I_k e^{j\omega_k t} = \sum_{n=-\infty}^{\infty} \sum_{m=-\infty}^{\infty} j\omega_{m+n} C_n V_m e^{j\omega_{m+n} t}. \quad (4.14)$$

A $j\omega$ term appears, as differentiation in the frequency domain is achieved by multiplication of $j\omega$. The conversion matrix form of this relation is

$$[I] = j[\Omega][C][V], \quad (4.15)$$

where $[\Omega]$ is the frequency conversion matrix from Figure 4.4.

$$\Omega = \begin{bmatrix} j\omega_{-N} & 0 & \dots & 0 \\ 0 & j\omega_{-N+1} & \dots & 0 \\ \dots & \dots & \dots & \dots \\ 0 & 0 & \dots & j\omega_N \end{bmatrix}$$

Figure 4.4: Omega conversion matrix for time-varying reactances from [23]

It is important to note however that the conversion matrix of the time-varying capacitance or inductance alone is of the same format as a time-varying resistance. The value of the reactance conversion matrix will then be seen in the format

$$j[\Omega][C] = \begin{bmatrix} j\omega_{-N} & 0 & 0 & \dots & 0 \\ 0 & j\omega_{-N+1} & 0 & \dots & \vdots \\ 0 & 0 & j\omega_{-N+2} & \dots & \vdots \\ \vdots & & & \ddots & \vdots \\ 0 & \dots & \dots & \dots & j\omega_N \end{bmatrix} \begin{bmatrix} C_0 & C_{-1} & C_{-2} & \dots & C_{-2N} \\ C_1 & C_0 & & & \vdots \\ C_2 & & \ddots & & \vdots \\ \vdots & & & \ddots & \vdots \\ C_{2N} & C_{2N-1} & \dots & \dots & C_0 \end{bmatrix} \quad (4.16)$$

4.3 Circuit Analysis with Conversion Matrices

Once each component has a corresponding conversion matrix, analysis of circuits with time-varying elements becomes relatively simple. One of the main benefits of conversion matrices is the fact that mathematical operations stay the same when circuit analysis is performed with them. This section will cover the steps of circuit analysis with conversion matrices, as well as multiple examples with one provided by [23]. All examples will follow a similar order of operations: first convert each of the components into its own individual conversion matrix, then combine compo-

nents as expected using mathematical relation of basic circuit analysis.

The first example of the conversion matrices applied to time-varying circuits is composed of three components shown in Figure 4.5: a static resistor R_a , and two time-varying resistances $R_b(t)$ and $R_c(t)$. As stated before, the first step in analyzing the time-varying circuit with the implementation of conversion matrices is to create the conversion matrix for each of the individual components. For this specific example, the resulting conversion matrices are:

$$[R_a] = \begin{bmatrix} R_a & 0 & 0 & \dots & 0 \\ 0 & R_a & 0 & \dots & \vdots \\ 0 & 0 & R_a & \dots & \vdots \\ \vdots & & & \ddots & \vdots \\ 0 & \dots & \dots & \dots & R_a \end{bmatrix}, \quad [R_b] = \begin{bmatrix} R_{b_0} & R_{b_{-1}} & R_{b_{-2}} & \dots & R_{b_{-2N}} \\ R_{b_1} & R_{b_0} & & & \vdots \\ R_{b_2} & & \ddots & & \vdots \\ \vdots & & & \ddots & \vdots \\ R_{b_{2N}} & R_{b_{2N-1}} & \dots & \dots & R_{b_0} \end{bmatrix},$$

$$\text{and } [R_c] = \begin{bmatrix} R_{c_0} & R_{c_{-1}} & R_{c_{-2}} & \dots & R_{c_{-2N}} \\ R_{c_1} & R_{c_0} & & & \vdots \\ R_{c_2} & & \ddots & & \vdots \\ \vdots & & & \ddots & \vdots \\ R_{c_{2N}} & R_{c_{2N-1}} & \dots & \dots & R_{c_0} \end{bmatrix}.$$

Once the matrices have been created, basis principles of circuit analysis can be applied to understand how they interact with each other. For this specific schematic, the total seen impedance $[Z]$ at the terminals can be described by the following equation

$$[Z] = [R_a] + ([R_b]^{-1} + [R_c]^{-1})^{-1} \quad (4.17)$$

where each value is the individual conversion matrices described before. This equation can then be expanded and observed in matrix form as the following:

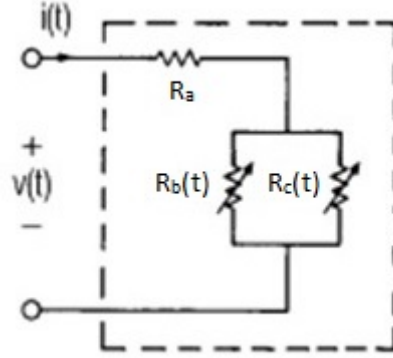


Figure 4.5: Example circuit to be solved with conversion matrices

$$\mathbf{Z} = \begin{bmatrix} R_a & 0 & 0 & \dots & 0 \\ 0 & R_a & 0 & \dots & \vdots \\ 0 & 0 & R_a & \dots & \vdots \\ \vdots & & & \ddots & \vdots \\ 0 & \dots & \dots & \dots & R_a \end{bmatrix} + \left(\begin{bmatrix} R_{b_0} & R_{b_{-1}} & R_{b_{-2}} & \dots & R_{b_{-2N}} \\ R_{b_1} & R_{b_0} & & & \vdots \\ R_{b_2} & & \ddots & & \vdots \\ \vdots & & & \ddots & \vdots \\ R_{b_{2N}} & R_{b_{2N-1}} & \dots & \dots & R_{b_0} \end{bmatrix}^{-1} + \begin{bmatrix} R_{c_0} & R_{c_{-1}} & R_{c_{-2}} & \dots & R_{c_{-2N}} \\ R_{c_1} & R_{c_0} & & & \vdots \\ R_{c_2} & & \ddots & & \vdots \\ \vdots & & & \ddots & \vdots \\ R_{c_{2N}} & R_{c_{2N-1}} & \dots & \dots & R_{c_0} \end{bmatrix}^{-1} \right)^{-1} \quad (4.18)$$

The second example, while having the same structure now introduces a time-varying capacitance, $C_j(t)$, and time-varying conductance, $g_j(t)$. Just as the previous example, the first step is to format the conversion matrices for each component where

$$[R] = \begin{bmatrix} R & 0 & 0 & \dots & 0 \\ 0 & R & 0 & \dots & \vdots \\ 0 & 0 & R & \dots & \vdots \\ \vdots & & & \ddots & \vdots \\ 0 & \dots & \dots & \dots & R \end{bmatrix}, \quad [C_j] = \begin{bmatrix} C_{j_0} & C_{j_{-1}} & C_{j_{-2}} & \dots & C_{j_{-2N}} \\ C_{j_1} & C_{j_0} & & & \vdots \\ C_{j_2} & & \ddots & & \vdots \\ \vdots & & & \ddots & \vdots \\ C_{j_{2N}} & C_{j_{2N-1}} & \dots & \dots & C_{j_0} \end{bmatrix},$$

$$\text{and } [G_j] = \begin{bmatrix} G_{j_0} & G_{j_{-1}} & G_{j_{-2}} & \cdots & G_{j_{-2N}} \\ G_{j_1} & G_{j_0} & & & \vdots \\ G_{j_2} & & \ddots & & \vdots \\ \vdots & & & \ddots & \vdots \\ G_{j_{2N}} & G_{j_{2N-1}} & \cdots & \cdots & G_{j_0} \end{bmatrix}.$$

Once this has been completed, the same circuit analysis can be performed. The equation for the total impedance $[Z]$ of this example slightly differs as it now includes the conversion matrix of a time-varying reactance.

$$[Z] = [R] + ([G_j] + j[\Omega][C_j])^{-1} \quad (4.19)$$

This equation can once again be expanded into matrix form as the following equation.

$$\mathbf{Z} = \begin{bmatrix} R_a & 0 & 0 & \cdots & 0 \\ 0 & R_a & 0 & \cdots & \vdots \\ 0 & 0 & R_a & \cdots & \vdots \\ \vdots & & & \ddots & \vdots \\ 0 & \cdots & \cdots & \cdots & R_a \end{bmatrix} + \left(\begin{bmatrix} G_{j_0} & G_{j_{-1}} & G_{j_{-2}} & \cdots & G_{j_{-2N}} \\ G_{j_1} & G_{j_0} & & & \vdots \\ G_{j_2} & & \ddots & & \vdots \\ \vdots & & & \ddots & \vdots \\ G_{j_{2N}} & G_{j_{2N-1}} & \cdots & \cdots & G_{j_0} \end{bmatrix} + \begin{bmatrix} j\omega_{-N} & 0 & 0 & \cdots & 0 \\ 0 & j\omega_{-N+1} & 0 & \cdots & \vdots \\ 0 & 0 & j\omega_{-N+2} & \cdots & \vdots \\ \vdots & & & \ddots & \vdots \\ 0 & \cdots & \cdots & \cdots & j\omega_N \end{bmatrix} \begin{bmatrix} C_{j_0} & C_{j_{-1}} & C_{j_{-2}} & \cdots & C_{j_{-2N}} \\ C_{j_1} & C_{j_0} & & & \vdots \\ C_{j_2} & & \ddots & & \vdots \\ \vdots & & & \ddots & \vdots \\ C_{j_{2N}} & C_{j_{2N-1}} & \cdots & \cdots & C_{j_0} \end{bmatrix} \right)^{-1} \quad (4.20)$$

4.3.1 Nodal Analysis

Conversion matrices and their extension to nodal analysis explained in [23] was the catalyst towards expanding their use to method of moment applications with antennas. Maas describes the applications of conversion matrices to nodal analysis as a way to create a "general-purpose circuit analysis program". This nodal analysis is described by defining two specific nodes i and j that contains some time-varying

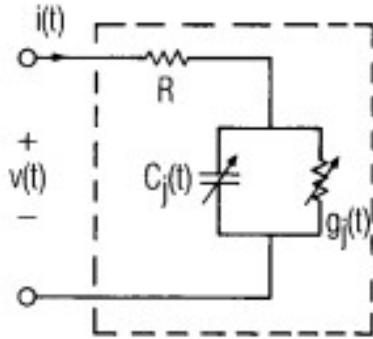


Figure 4.6: Example circuit for conversion matrix analysis from [23]

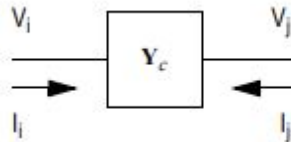


Figure 4.7: Two node network from [23]

admittance between the two with a conversion matrix Y_c . Maas then treats this pair of nodes as a two-port network. A visualization of a network between two nodes can be found in Figure 4.7. This nodal analysis using conversion matrices is not restricted to circuits of a two nodes however. A nodal matrix is simply formed where each element uses conversion matrices to describe the interaction between each of the different nodes in the circuit. This expanded node matrix can be seen in Figure 4.8.

$$\begin{bmatrix} \dots \\ \mathbf{I}_i \\ \mathbf{I}_j \\ \dots \\ \dots \end{bmatrix} = \begin{bmatrix} \dots & \dots & \dots & \dots & \dots \\ \dots & \dots + \mathbf{Y}_c & \dots - \mathbf{Y}_c & \dots & \dots \\ \dots & \dots - \mathbf{Y}_c & \dots + \mathbf{Y}_c & \dots & \dots \\ \dots & \dots & \dots & \dots & \dots \\ \dots & \dots & \dots & \dots & \dots \end{bmatrix} \begin{bmatrix} \dots \\ \mathbf{V}_i \\ \mathbf{V}_j \\ \dots \\ \dots \end{bmatrix}$$

Figure 4.8: Nodal matrix for system of greater than two nodes from [23]

4.4 Summary

Conversion matrices as described by [23] are an incredibly useful tool when applied to analyzing circuits with time-varying components. Once formatted correctly, they can be applied to a wide variety of circuit applications in many forms. This project will utilize that flexibility, and the ability for conversion matrices to describe the voltage to current relation for a variety of frequencies. While this chapter covered the basis of conversion matrices and their possible uses, the next chapter will diver deeper into their application to antennas.

Chapter 5

Conversion Matrices Antenna Applications

This chapter will cover the application of conversion matrices as a technique for understanding the behavior of time-varying loads on antennas. While their use for this application has been seen before, this section will propose an expansion of the technique that is capable of surpassing the limitations of the previous techniques. The chapter will conclude with a comparison of the performance of the techniques to the time-domain Landt Integral Method.

5.1 Past Conversion Matrix Antenna Application

Due to their utility in analyzing time-varying circuits, it is intuitive to apply the same theory of conversion matrices towards the application of time-varying loads on antennas. Examples of applications of conversion matrices to antennas are introduced by both Huang and Flaviis in [22], [24]. These papers present the application to model not only time-varying resistors, but capacitive switches as well. Both are based off the description of the loaded antenna as an equivalent circuit, but slightly differ from each other based off the utilized components and setup of the load.

The first of the examples to be discussed is from Huang in [22]. Huang introduces a combination of harmonic balance and method of moments in order to

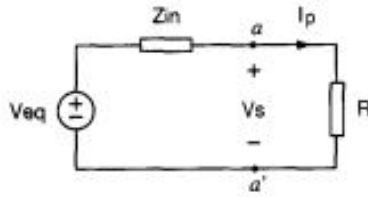


Figure 5.1: Equivalent circuit used by [22] to apply conversion matrices to antennas

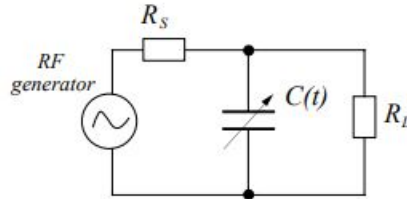


Figure 5.2: Equivalent circuit used by [24] to describe capacitive switches on antenna

analyze not only nonlinear but also time-varying loads on antennas. The equivalent circuit used to represent the loaded antenna is shown in Figure 5.1. In the equivalent circuit, the value of Z_{in} represents the input impedance of the antenna at the loaded location. The value R represents the time-varying resistive load; however, it is mentioned that this value can be replaced with that of a time-varying capacitance or inductance with the proper measures as covered in the previous chapter. The second example, while having a differing equivalent circuit layout, follows the same methodology. This example from [24] investigates the applications of capacitive switches to antennas. Conversion matrices applied to basic circuit analysis are used to solve these equivalent circuits and find the currents on the load.

5.1.1 Setbacks with Previous Work

The application of conversion matrices to antennas as shown by [22], [24] have two primary restrictions: the capability of only a single observation point, and a single time-varying load. By design, the equivalent circuit assumed that the input

impedance itself was a static component, only varying by frequency. It did not account for the ability to understand what a time-varying load may look like from an observation point located on the other end of the antenna. This lack of differing observation points led to the inability to apply multiple time-varying loads. Without being able to understand how a time-varying load would affect a different observation point, it was also not capable at understanding how a time-varying load would affect another at a different location.

For this project, it was important to have the freedom to apply multiple time-varying loads to a variety of locations, as well as see the current distribution at all points on the antenna. Restrictions on the previously proposed applications of conversion matrices is based off the characterization of the antenna as an equivalent circuit. Characterizing an entire antenna as a single impedance value that is then loaded was not capable of providing the generalization the project aimed for.

5.2 Expansion to Harrington Method of Moments

The methods introduced in [22], [24] were restricted based on the antenna being modeled as an equivalent circuit. In order to move past such restrictions, an expansion was made to apply conversion matrices more broadly to the full impedance matrix of an antenna. Instead of creating conversion matrices of single element values, such as the input impedance of the loaded point, a much larger conversion matrix can be made to describe the impedance of the whole antenna and its behavior at multiple mixing frequencies. This was seen as an intuitive next step, utilizing the nodal analysis method introduced in [23], but applying it to a method of moments extracted impedance matrix. With this expansion, many of the principles from [20] can be applied to antennas with time-varying loads, including the capability of an-

alyzing multiple loads from various observation points. This section will cover this expansion of matrices, as well as its implementation for antenna analysis.

5.2.1 Impedance Conversion Matrix

The first and most important expansion made with conversion matrices is that of the unloaded impedance matrix of the antenna in use. For ease of explanation, the expansion will be described in terms of a simple dipole antenna. As covered in Chapter 2, the method of moments extraction of an impedance matrix utilizing a pulse basis function will return an $N \times N$ impedance matrix, where N corresponds to the number of segments the antenna is separated into. For example, a thin wire dipole antenna separated into three segments as seen in Figure 5.3 will result in a 3×3 impedance matrix of the format

$$[Z] = \begin{bmatrix} z_{11} & z_{12} & z_{13} \\ z_{21} & z_{22} & z_{23} \\ z_{31} & z_{32} & z_{33} \end{bmatrix}. \quad (5.1)$$

The diagonal elements of this matrix represent the self impedances of the segments on the antenna, and all other elements represent the interaction impedances between segments. This extracted impedance matrix however is dependent on the frequency at which the antenna is operating at, which is an important factor when creating the impedance conversion matrix for the entire antenna.

As stated in the previous chapter, the conversion matrix of a static component is a diagonal matrix where each element corresponds to the value of the component at a different mixing frequency. In order to convert the typical antenna impedance matrix into its conversion matrix form, the first step is to identify the number of



Figure 5.3: Example of wire antenna separated into three segments

mixing frequencies one wishes to observe. For simplicity in this example, we will begin with just the signal frequency ω_s , and the first positive and negative mixing frequencies, $\omega_{+1} = \omega_s + \omega_n$ and $\omega_{-1} = \omega_s - \omega_n$ respectively. It is important to note once again the mixing frequency is defined by the relation

$$\omega_n = \omega_s + n\omega_p \quad (5.2)$$

where ω_p is the frequency the load is modulating. By specifying that only 3 mixing frequencies, $n = -1, 0, 1$, will be observed, the resulting impedance conversion matrix will be a 3×3 impedance matrix comprised of 3×3 conversion matrices, resulting in a 9×9 total matrix size. Each individual element in the original impedance will be expanded to a conversion matrix defined by the given mixing frequencies. For example, the z_{11} element will be expanded to

$$z_{11} \implies \begin{bmatrix} z_{11}(\omega_{-1}) & 0 & 0 \\ 0 & z_{11}(\omega_0) & 0 \\ 0 & 0 & z_{11}(\omega_{+1}) \end{bmatrix}. \quad (5.3)$$

When this extension is applied to all elements of the original impedance matrix, the expanded impedance matrix can be viewed as

$$\begin{bmatrix} z_{11} & z_{12} & z_{13} \\ z_{21} & z_{22} & z_{23} \\ z_{31} & z_{32} & z_{33} \end{bmatrix} \Rightarrow \begin{bmatrix} \begin{bmatrix} z_{11}(\omega_{-1}) & 0 & 0 \\ 0 & z_{11}(\omega_0) & 0 \\ 0 & 0 & z_{11}(\omega_{+1}) \end{bmatrix} & \begin{bmatrix} z_{12}(\omega_{-1}) & 0 & 0 \\ 0 & z_{12}(\omega_0) & 0 \\ 0 & 0 & z_{12}(\omega_{+1}) \end{bmatrix} & \begin{bmatrix} z_{13}(\omega_{-1}) & 0 & 0 \\ 0 & z_{13}(\omega_0) & 0 \\ 0 & 0 & z_{13}(\omega_{+1}) \end{bmatrix} \\ \begin{bmatrix} z_{21}(\omega_{-1}) & 0 & 0 \\ 0 & z_{21}(\omega_0) & 0 \\ 0 & 0 & z_{21}(\omega_{+1}) \end{bmatrix} & \begin{bmatrix} z_{22}(\omega_{-1}) & 0 & 0 \\ 0 & z_{22}(\omega_0) & 0 \\ 0 & 0 & z_{22}(\omega_{+1}) \end{bmatrix} & \begin{bmatrix} z_{23}(\omega_{-1}) & 0 & 0 \\ 0 & z_{23}(\omega_0) & 0 \\ 0 & 0 & z_{23}(\omega_{+1}) \end{bmatrix} \\ \begin{bmatrix} z_{31}(\omega_{-1}) & 0 & 0 \\ 0 & z_{31}(\omega_0) & 0 \\ 0 & 0 & z_{31}(\omega_{+1}) \end{bmatrix} & \begin{bmatrix} z_{32}(\omega_{-1}) & 0 & 0 \\ 0 & z_{32}(\omega_0) & 0 \\ 0 & 0 & z_{32}(\omega_{+1}) \end{bmatrix} & \begin{bmatrix} z_{33}(\omega_{-1}) & 0 & 0 \\ 0 & z_{33}(\omega_0) & 0 \\ 0 & 0 & z_{33}(\omega_{+1}) \end{bmatrix} \end{bmatrix} \quad (5.4)$$

This expanded impedance matrix is the basis of the expansions made to conversion matrices and their application to antennas. It allows for the principles introduced by [20] to be applied, and therefore a generalization in the Conversion Matrices Method for analyzing time-varying loads on antennas.

5.2.2 Loading the Conversion Matrix

Due to the expansion of the impedance matrix, loading the antenna as shown in Chapter 2 can be performed even with the presence of time-varying loads. For a continuation of the three segmented dipole, the center segment will now be loaded

with a time-varying resistance shown in Figure 5.4. The first step is to identify the conversion matrix for the time-varying load. For this example, the resulting conversion matrix is shown as

$$\mathbf{R} = \begin{bmatrix} R_0 & R_{-1} & R_{-2} \\ R_1 & R_0 & R_{-1} \\ R_2 & R_1 & R_0 \end{bmatrix}. \quad (5.5)$$

Once the conversion matrix for the load is created, it can be applied to the impedance conversion matrix using the same techniques as Harrington. The value of the load is subtracted from the self impedance of the segment that the load is located on. This subtraction is due to the previously mentioned reference conditions stated by Harrington

$$v_i = -Z_L i_i, \quad (5.6)$$

where v_i and i_i are voltage and current on the loaded segment respectively. A representation of this principle being applied to the impedance conversion matrix is shown in (5.7). This is now the total loaded impedance matrix that can then be used with an excitation matrix.



Figure 5.4: Example of wire antenna now with the addition of a time-varying load

$$\begin{bmatrix} z_{11} & z_{12} & z_{13} \\ z_{21} & z_{22} - \mathbf{R} & z_{23} \\ z_{31} & z_{32} & z_{33} \end{bmatrix} \Rightarrow \begin{bmatrix} \begin{bmatrix} z_{11}(\omega_{-1}) & 0 & 0 \\ 0 & z_{11}(\omega_0) & 0 \\ 0 & 0 & z_{11}(\omega_{+1}) \end{bmatrix} & \begin{bmatrix} z_{12}(\omega_{-1}) & 0 & 0 \\ 0 & z_{12}(\omega_0) & 0 \\ 0 & 0 & z_{12}(\omega_{+1}) \end{bmatrix} & \begin{bmatrix} z_{13}(\omega_{-1}) & 0 & 0 \\ 0 & z_{13}(\omega_0) & 0 \\ 0 & 0 & z_{13}(\omega_{+1}) \end{bmatrix} \\ \begin{bmatrix} z_{21}(\omega_{-1}) & 0 & 0 \\ 0 & z_{21}(\omega_0) & 0 \\ 0 & 0 & z_{21}(\omega_{+1}) \end{bmatrix} & \begin{bmatrix} z_{22}(\omega_{-1}) - R_0 & -R_{-1} & -R_{-2} \\ -R_1 & z_{22}(\omega_0) - R_0 & -R_{-1} \\ -R_2 & -R_1 & z_{22}(\omega_{+1}) - R_0 \end{bmatrix} & \begin{bmatrix} z_{23}(\omega_{-1}) & 0 & 0 \\ 0 & z_{23}(\omega_0) & 0 \\ 0 & 0 & z_{23}(\omega_{+1}) \end{bmatrix} \\ \begin{bmatrix} z_{31}(\omega_{-1}) & 0 & 0 \\ 0 & z_{31}(\omega_0) & 0 \\ 0 & 0 & z_{31}(\omega_{+1}) \end{bmatrix} & \begin{bmatrix} z_{32}(\omega_{-1}) & 0 & 0 \\ 0 & z_{32}(\omega_0) & 0 \\ 0 & 0 & z_{32}(\omega_{+1}) \end{bmatrix} & \begin{bmatrix} z_{33}(\omega_{-1}) & 0 & 0 \\ 0 & z_{33}(\omega_0) & 0 \\ 0 & 0 & z_{33}(\omega_{+1}) \end{bmatrix} \end{bmatrix} \quad (5.7)$$

5.2.3 Excitation Matrix

Once the wire is loaded, the final step towards understanding the behavior of the antenna with a time-varying load is exciting the antenna. Similar to that of the impedance matrix, the excitation matrix is an expansion of that introduced by Harrington. As this project aimed to design a receive antenna, this section will primarily cover the introduction of an incident plane wave on the antenna. Exciting the antenna with a direct feed would be fairly intuitive with an expanded excitation matrix using methods from Harrington.

To continue the example for a three-segmented dipole, an incident E-field plane wave approaching the antenna at broadside will have the following matrix

$$[V] = \begin{bmatrix} E(t) * d \\ E(t) * d \\ E(t) * d \end{bmatrix}, \quad (5.8)$$

where $E(t) = E_0 * e^{j\omega_s t}$, ω_s is the signal frequency of the incident E-field, and $d = 2k\Delta^2$ where k is the propagation constant of the medium as discussed in Chapter 2. In order to account for a plane wave approaching the antenna at a differing incident angle, the value of $E(t)$ now becomes

$$E(t) = (E_0 * e^{j\omega_s t}) * \sin\theta * e^{jkz\cos\theta} \quad (5.9)$$

where z is the segment that $E(t)$ is being evaluated at and θ is the angle of incidence [26]. The matrix of a plane wave approaching the antenna can therefore be written

as

$$[V] = \begin{bmatrix} (E_0 * d * e^{j\omega_s t}) * \sin\theta e^{jkz\cos\theta} \\ (E_0 * d * e^{j\omega_s t}) * \sin\theta e^{jkz\cos\theta} \\ (E_0 * d * e^{j\omega_s t}) * \sin\theta e^{jkz\cos\theta} \end{bmatrix}. \quad (5.10)$$

In order to create the conversion matrices version of the excitation matrix, the element for each of the segments must be expanded based on the number of mixing frequencies being observed. For the purposes of this project, it was assumed that the plane wave was oscillating at a single frequency (ω_s). In the absence of any mixing frequencies in the incident E-field, the conversion matrix form is fairly simple. For a single segment, the time-varying E-field will have a conversion matrix form of

$$v(t) = (E_0 * d * e^{j\omega_s t}) * \sin\theta e^{jkz\cos\theta} \implies \begin{bmatrix} 0 \\ E_0 * d * \sin\theta e^{jkz\cos\theta} \\ 0 \end{bmatrix} \quad (5.11)$$

where zeros are observed at the elements for the mixing frequencies other than that of the fundamental signal frequency ω_s . In order to expand this matrix for the three segment dipole presented before, the resulting conversion matrices excitation matrix is

$$\begin{bmatrix} (E_0 * d * e^{j\omega_s t}) * \sin\theta e^{jkz\cos\theta} \\ (E_0 * d * e^{j\omega_s t}) * \sin\theta e^{jkz\cos\theta} \\ (E_0 * d * e^{j\omega_s t}) * \sin\theta e^{jkz\cos\theta} \end{bmatrix} \Rightarrow \begin{bmatrix} \begin{bmatrix} 0 \\ E_0 * d * \sin\theta e^{jkz\cos\theta} \\ 0 \end{bmatrix} \\ \begin{bmatrix} 0 \\ E_0 * d * \sin\theta e^{jkz\cos\theta} \\ 0 \end{bmatrix} \\ \begin{bmatrix} 0 \\ E_0 * d * \sin\theta e^{jkz\cos\theta} \\ 0 \end{bmatrix} \end{bmatrix} . \quad (5.12)$$

5.3 Current Distribution

This excitation conversion matrix can then be multiplied by the impedance matrix in order to find the current distribution on the antenna. This is done using the methods found once again from Harrington using the relation

$$[I] = [Y][V], \quad (5.13)$$

a method of moments matrix form of Ohm's law. $[Y]$ represents the loaded admittance matrix, or the inverse of the loaded impedance matrix in conversion matrix form created in the earlier section. The loaded admittance matrix is then multiplied by the conversion matrix excitation matrix to create the resulting current distribution. (5.14) shows a visualization of the complete conversion matrix form of the

impedance, excitation, and current distribution matrices.

$$\begin{aligned}
 & \begin{bmatrix} I_1(\omega_{-1}) \\ I_1(\omega_0) \\ I_1(\omega_{+1}) \end{bmatrix} = \begin{bmatrix} z_{11}(\omega_{-1}) & 0 & 0 \\ 0 & z_{11}(\omega_0) & 0 \\ 0 & 0 & z_{11}(\omega_{+1}) \end{bmatrix} \begin{bmatrix} z_{12}(\omega_{-1}) & 0 & 0 \\ 0 & z_{12}(\omega_0) & 0 \\ 0 & 0 & z_{12}(\omega_{+1}) \end{bmatrix} \begin{bmatrix} z_{13}(\omega_{-1}) & 0 & 0 \\ 0 & z_{13}(\omega_0) & 0 \\ 0 & 0 & z_{13}(\omega_{+1}) \end{bmatrix}^{-1} \begin{bmatrix} 0 \\ E_0 * d * \sin\theta * e^{jkz \cos\theta} \\ 0 \end{bmatrix} \\
 & \begin{bmatrix} I_2(\omega_{-1}) \\ I_2(\omega_0) \\ I_2(\omega_{+1}) \end{bmatrix} = \begin{bmatrix} z_{21}(\omega_{-1}) & 0 & 0 \\ 0 & z_{21}(\omega_0) & 0 \\ 0 & 0 & z_{21}(\omega_{+1}) \end{bmatrix} \begin{bmatrix} z_{22}(\omega_{-1}) - R_0 & -R_{-1} & -R_{-2} \\ -R_1 & z_{22}(\omega_0) - R_0 & -R_{-1} \\ -R_2 & -R_1 & z_{22}(\omega_{+1}) - R_0 \end{bmatrix} \begin{bmatrix} z_{23}(\omega_{-1}) & 0 & 0 \\ 0 & z_{23}(\omega_0) & 0 \\ 0 & 0 & z_{23}(\omega_{+1}) \end{bmatrix} \begin{bmatrix} 0 \\ E_0 * d * \sin\theta * e^{jkz \cos\theta} \\ 0 \end{bmatrix} \\
 & \begin{bmatrix} I_3(\omega_{-1}) \\ I_3(\omega_0) \\ I_3(\omega_{+1}) \end{bmatrix} = \begin{bmatrix} z_{31}(\omega_{-1}) & 0 & 0 \\ 0 & z_{31}(\omega_0) & 0 \\ 0 & 0 & z_{31}(\omega_{+1}) \end{bmatrix} \begin{bmatrix} z_{32}(\omega_{-1}) & 0 & 0 \\ 0 & z_{32}(\omega_0) & 0 \\ 0 & 0 & z_{32}(\omega_{+1}) \end{bmatrix} \begin{bmatrix} z_{33}(\omega_{-1}) & 0 & 0 \\ 0 & z_{33}(\omega_0) & 0 \\ 0 & 0 & z_{33}(\omega_{+1}) \end{bmatrix} \begin{bmatrix} 0 \\ E_0 * d * \sin\theta * e^{jkz \cos\theta} \\ 0 \end{bmatrix}
 \end{aligned} \tag{5.14}$$

Once the matrix multiplication is performed, the resulting current matrix is made of conversion matrices describing the frequency spectrum of the currents found on each of the individual segments. For the three segment example dipole, the resulting current matrix will be in the form,

$$\begin{bmatrix}
\begin{bmatrix} I_1(\omega_{-1}) \\ I_1(\omega_0) \\ I_1(\omega_{+1}) \end{bmatrix} \\
\begin{bmatrix} I_2(\omega_{-1}) \\ I_2(\omega_0) \\ I_2(\omega_{+1}) \end{bmatrix} \\
\begin{bmatrix} I_3(\omega_{-1}) \\ I_3(\omega_0) \\ I_3(\omega_{+1}) \end{bmatrix}
\end{bmatrix}, \quad (5.15)$$

where the 4th through 6th elements are extracted to find the current on the load. Figure 5.5 shows the current magnitude values for the three mixing frequencies from the matrix being plotted in order to represent the current spectrum. In order to see the current spectrum at differing observations points, the element values that correspond to the conversion matrix for that specific segment are extracted.

5.4 Comparison of Performance

In order to test the validity of the Conversion Matrices method, it must be compared to known methods. The main standard for performance of the Conversion Matrices Method is the comparison of its results to those obtained using the Landt Integral Method. This section will cover the results of the Landt Integral Method and Conversion matrices method with an example that was first presented by Landt and covered in Chapter 3. This was also the example used to confirm the performance

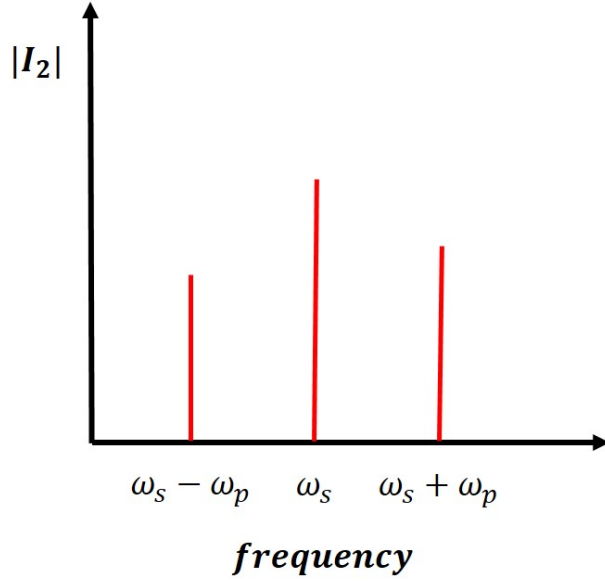


Figure 5.5: The current spectrum from the extracted conversion matrix

of Huang’s method. To reiterate, the example is a dipole 9 m in length and 0.2 m in radius. The dipole is divided into 9 segments and center loaded with a time-varying resistance of the value

$$R(t) = 500(1 + \sin(\omega_p t)) \Omega \quad (5.16)$$

where $\omega_p = 2\pi(4 \text{ MHz})$. An incident wave is approaching the antenna oscillating at $\omega_s = 2\pi(16 \text{ MHz})$ and a magnitude of $E_0 = 1 \text{ V/m}$. The results in this chapter will also be presented as the magnitude of the current spectrum on the antenna, just as they were in Chapter 3.

5.4.1 Base Results

Results of the Landt Integral Method for the same example were pulled from Chapter 3. The base results found using both the Landt Integral Method and Conver-

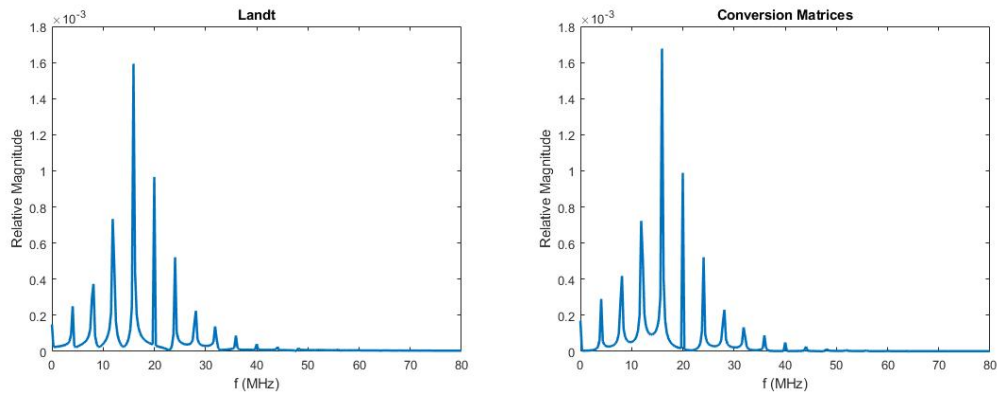


Figure 5.6: Result of current spectrum from Landt Integral Method and comparison to result from Conversion Matrices Method

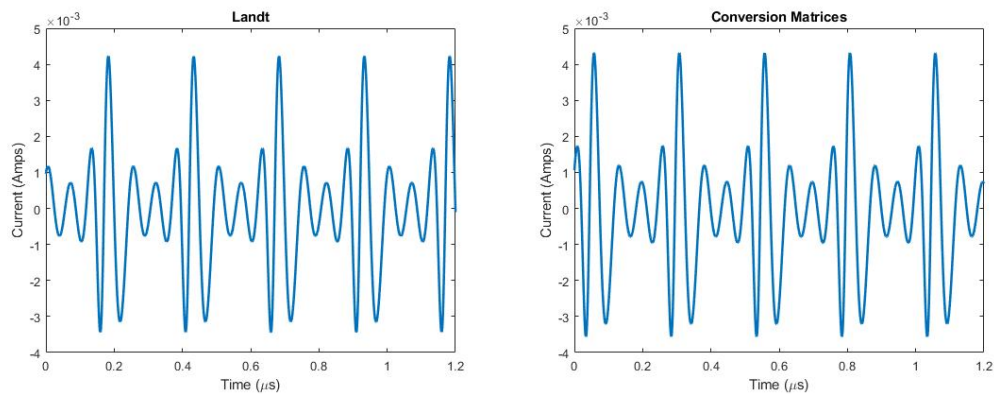


Figure 5.7: Result of current waveform from both Landt Integral Method and Conversion Matrices Method

Conversion Matrices Method were then compared in Figure 5.6. The two plots show great agreement, with only slight variations in magnitude and spectrum shape. The waveform shape is also consistent between the two methods. Figure 5.7 shows the current waveform at the feed point obtained using the MATLAB replication of the Landt Integral Method and Conversion Matrices Method. The only discrepancy between the two is a slight phase shift, but the waveform itself is in line between the two methods.

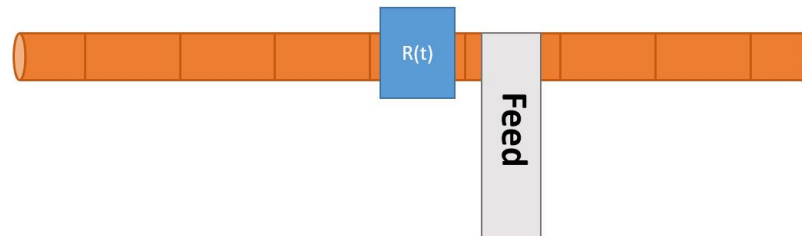


Figure 5.8: Visualization of an example used to test the results of differing feed locations using Conversion Matrices Method

5.4.2 Varying Locations

As previously mentioned, one of the restrictions of conversion matrices and their applications to antennas using an equivalent circuit was the inability to analyze the currents anywhere else except on the load. This section will cover the performance of the Conversion Matrices Method and its ability to match up to the Landt Integral Method at a variety of observation points along the antenna. In order to do so, the Landt Integral Method and Conversion Matrices Method were both used to analyze the same antenna from the previous example, where instead the feed is located one segment away from the load. The setup used in this example is shown in Figure 5.8.

Figure 5.9 shows the results for both methods. There is a very apparent decrease in the magnitudes of the mixing frequencies, and an increase of the main fundamental frequency at 16 MHz. These results show good agreement once again between the two methods, and shows that the expansion of the conversion matrices for antennas allows for accurate analysis at feed points other than the load location.

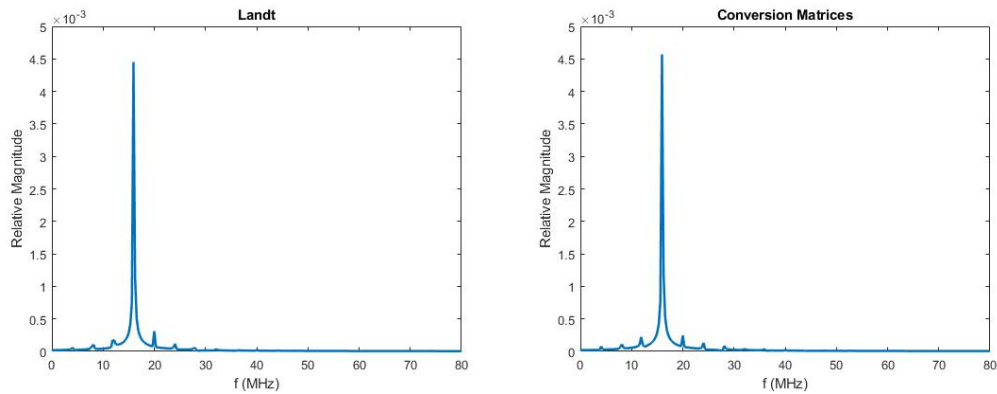


Figure 5.9: Results from the Landt Integral Method and Conversion Matrices Method one segment away from the load

5.4.3 Multiple Loads

The second restriction presented in the previous applications of conversion matrices was the inability to place multiple time-varying loads in arbitrary locations. To test the ability of the Conversion Matrices Method to match the Landt Integral Method solutions with multiple loads, the following example was simulated. The same dipole from the base example was used, which has a central load with a time-varying resistance. Just like the example proving the validity of the Conversion Matrices Method at differing observation locations, the feed was placed one segment away from the center. This time however, the load at the center was duplicated and placed one segment over from the feed, leaving the feed settled in between two time-varying loads. A visualization of this example is shown in Figure 5.10. The incident wave properties, dimensions of the antenna, and time-varying resistances are identical to the base example provided at the beginning of this section.

The results of this simulation using the Landt Integral Method and Conversion Matrices Method are shown in Figure 5.11. It is first important to note that both results show great similarities to each other, confirming the belief that the Conver-

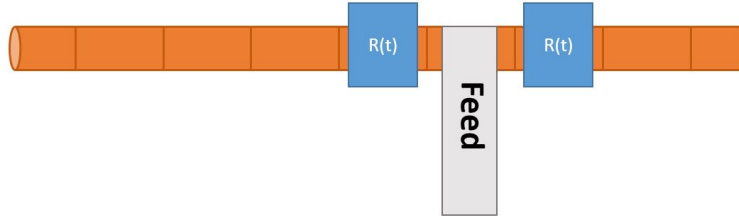


Figure 5.10: Visualization of example used to test the results of multiple loads using the Conversion Matrices Method

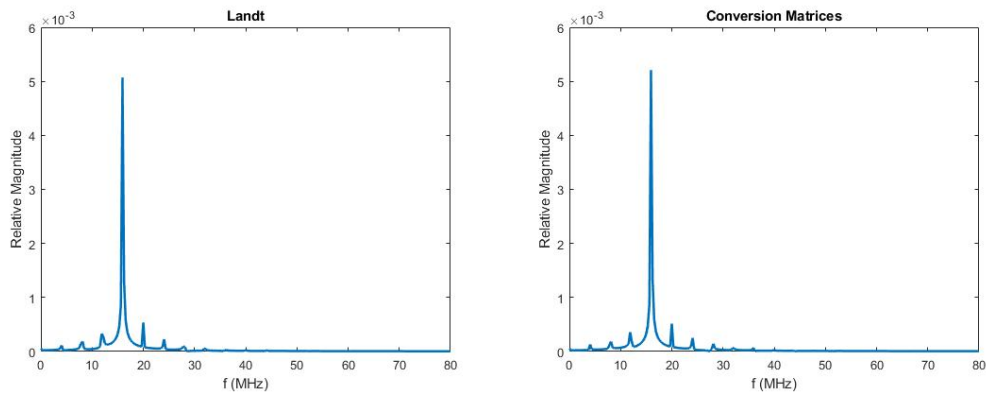


Figure 5.11: Comparison of the Landt and Conversion Matrices methods for a dipole antenna with two time-varying resistances and single feed point all located at different locations

sion Matrices Method can model multiple loads just like the Landt Integral Method. This solves the second concern that was brought up with the original application of conversion matrices to antennas with time-varying loads. Additionally, the application of a second time-varying load to the antenna shows a greater magnitude of current being received at the feed than in the example in the section testing simply feed locations differing from the load. This is also with fairly little change to the actual shape of the current spectrum itself other than a slight increase in mixing frequency magnitudes.

5.5 Summary

This chapter showed the introduction of an expanded conversion matrices method to analyze time-varying loads on antennas. This method utilizes conversion matrices in the creation of a new impedance matrix, rather than confining itself to equivalent circuits that describe the antenna. This new form of impedance matrix and electromagnetic computation dismisses the restraints on previous applications of conversion matrices to antennas. The introduced Conversion Matrices Method provides the ability to handle both multiple time-varying loads, as well as differing observation points. The next chapter will discuss a generalization of this method and its application using extracted impedance matrices from an electromagnetic solver method of moments solver.

Chapter 6

Generalization of the Conversion Matrices Method

In order to take the Conversion Matrix Method and make it capable of widespread use for varying types of antennas, the capability to extract the impedance matrix for a broad range of antennas is imperative. It is known that as the structure of an antenna moves beyond a thin wire and to more complicated geometries, the method of moments computation of the impedance matrix becomes increasingly more intensive. In order to reduce computational work, but still expand the variety of antennas this method could be applied to, it was seen as valuable to make the method compatible with impedance matrices extracted from a computational electromagnetics solver that utilizes method of moments. FEKO by Altair Engineering, which comes from the German phrase that roughly translates to “field calculations involving bodies of arbitrary shape”, is a software that solves for the fields and characteristics of a component by meshing the structure and using method of moments based off Maxwell’s equations. For this thesis, the FEKO software is used to validate methodology and provide a proof-of-concept example. This chapter will cover a brief overview of the basis functions used by FEKO for the method of moments calculations, wire and planar structures in FEKO, and results of implementing the Conversion Matrices Method with FEKO impedance matrices.

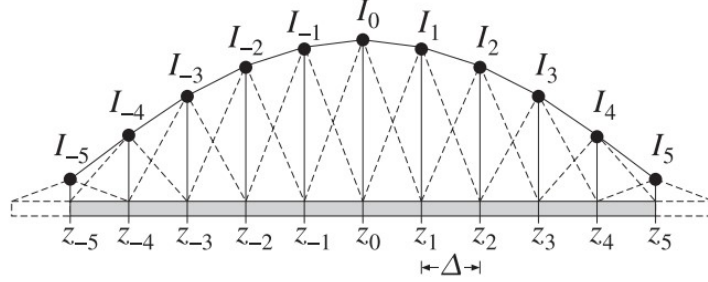


Figure 6.1: Representation of piecewise triangular basis function from [26] that is used by FEKO

6.1 Wire Meshing

In FEKO, the meshing and computation of a thin wire antenna is fairly simple. While a pulse basis function creates a constant value for a single segment on the wire, FEKO uses instead a piecewise triangular basis function, observing the interaction between two segments. Therefore, rather than a value for a self impedance being identified on a single segment, it is assigned to the edge between the two segments it represents. A visualization of the basis function used by FEKO is shown in Figure 6.1 and was covered in depth in Chapter 2. Due to the application to thin wire antennas, the assumption of zero current can be made for the end values of I_{-M} and I_{+M} . This is why when the impedance matrix is extracted from FEKO, there are no element values for the “edge” or end of the antenna. For example, an antenna divided into 10 segments will return a 9×9 impedance matrix instead of 11×11 .

6.1.1 Thin Wire Dipole

The modeling of a thin wire dipole in FEKO is considered one of the most simple geometries and provides a good starting point for the implementation of the Conversions Matrices Method using FEKO generated impedance matrices. The

example used in the prior chapters of a 9 m long dipole centrally fed was once again used; however, the dipole was instead separated into 10 segments. An even number of segments was required as now instead of loading the impedance matrix element that corresponded to the central segment, the element of the edge between two central segments was loaded. The 10 equally sized segments allowed for the extracted impedance matrix elements to correspond to the 9 interior edges. The antenna model used is shown in Figure 6.2. The time-varying resistance as well as the incident wave are the same as the base example from the prior chapters as well. FEKO does not allow for negative frequencies to be solved for, and because there must be an equal number of positive and negative mixing frequencies that the impedance matrices are solved for, the zero frequency limit acted as a barrier. An attempt was made to have FEKO simulate the negative frequencies, but the error message “Error 17505: Parameter should be > 0 for parameter” was the response. Due to this barrier, FEKO solved for only 4 negative and 4 positive mixing frequencies before the negative mixing frequencies hit the zero barrier. This resulted in a total of 9 evaluated frequencies including f_s .

The setup of the initial test done with a FEKO impedance matrix is shown in Figure 6.3. The results of the current spectrum evaluated on the center load using the Landt Integral Method and Conversion Matrices Method with the FEKO extracted impedance matrix are shown in Figure 6.4. While the spectrum shape varies slightly more than the results from the MATLAB calculated impedance matrices, the magnitudes of the current spectrums and general shape still show good agreement. This discrepancy is partially assumed to be due to the restriction on number of mixing frequencies that could be evaluated. Despite the results for this specific example, multiple other orientations were tested in order to further validate that the methods still reflected each other in more cases.

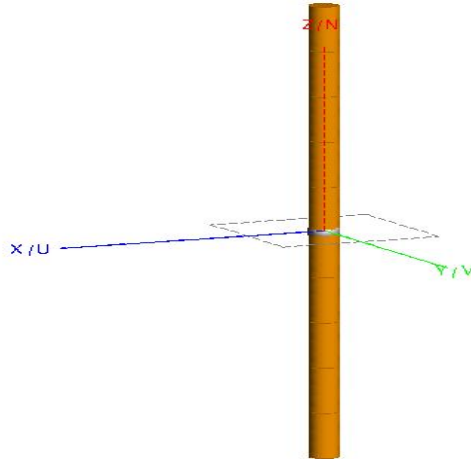


Figure 6.2: Simulated model in FEKO for wire antenna, separated into 10 segments with 9 edges between segments

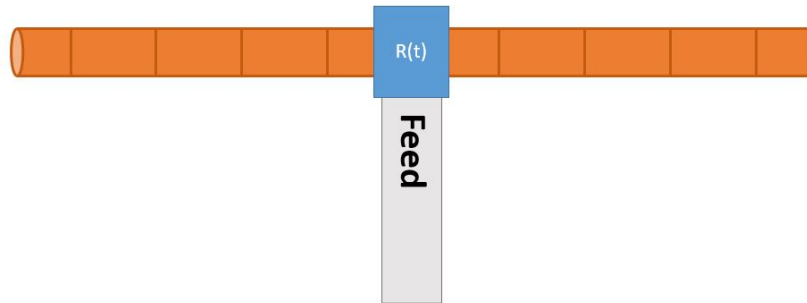


Figure 6.3: Setup of simulation done for FEKO extracted wire antenna impedance matrix with load and feed at the center of the dipole

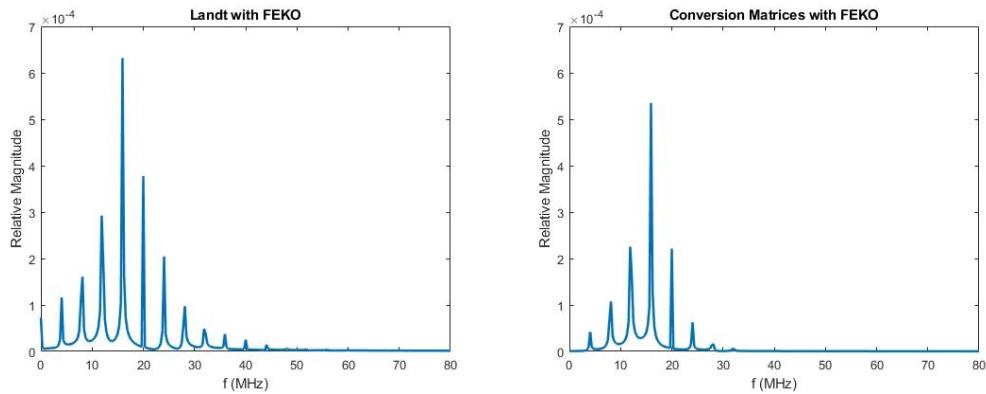


Figure 6.4: Results of current spectrum on the central load from Landt Integral Method and Conversion Matrices Method using FEKO extracted impedance matrix of a wire antenna

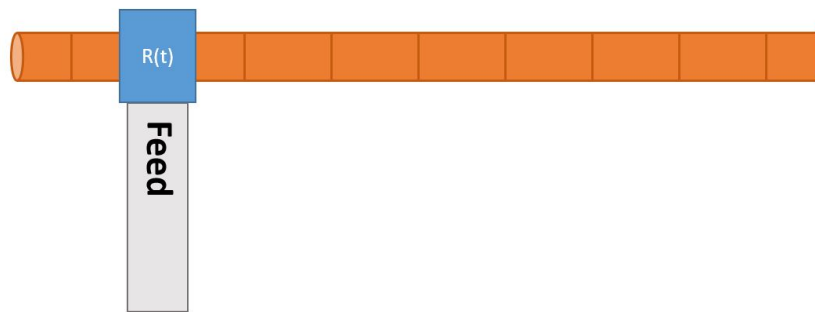


Figure 6.5: Setup of simulation done for FEKO extracted wire antenna impedance matrix with load on the second edge between segments

When the load was moved away from the center, the methods showed even more agreement. In order to once again test the versatility of the method, the load was moved from the center to the second edge between the second and third segment from the antenna end as shown in Figure 6.5. The feed however was kept to be at the same location as the load. The results of this example, shown in Figure 6.6 were even more promising as the current spectrums matched very well.

In order to test the location of the feed at a differing location other than at the load, the feed was moved back to the center of the antenna. The configuration

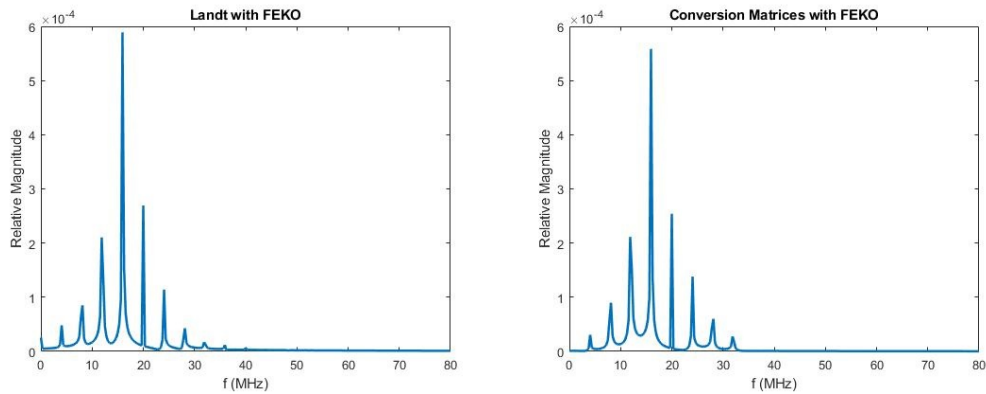


Figure 6.6: Result of the current spectrum on the load from Landt Integral Method and Conversion Matrices Method using FEKO extracted impedance matrix of a wire antenna with the load moved to the second edge from the end of the antenna

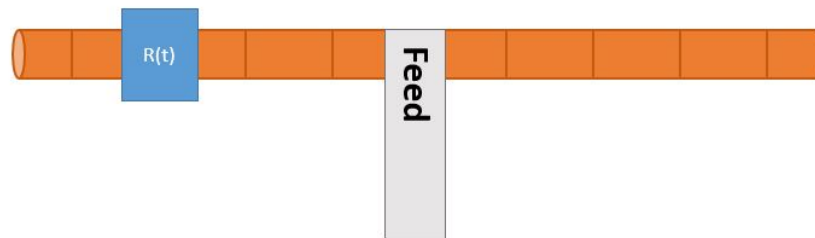


Figure 6.7: Setup of simulation done for FEKO extracted wire antenna impedance matrix to test feed points away from the load

for this test is shown in Figure 6.7. The results in Figure 6.8 show a decrease in harmonic prominence compared to the magnitude of the fundamental frequency. There was also an increase in the magnitude of the fundamental frequency current which was expected, as the feed was placed at the center of the dipole and less affected by the modulation of the load.

The FEKO extracted impedance matrices were then tested for the application of multiple loads. A second time-varying resistance was placed proportionally on the other side of the antenna from the feed as shown in Figure 6.9. In terms of edge number, the loads were placed on the 2nd and 8th edge, and the feed at the

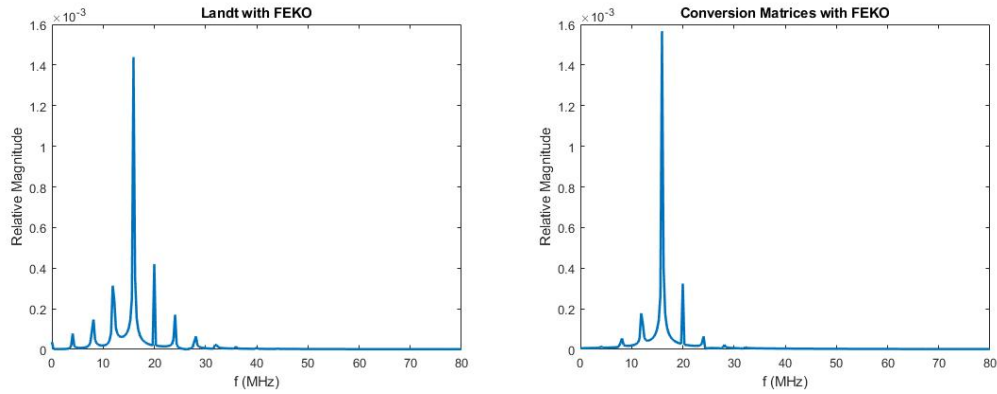


Figure 6.8: Result of current spectrum on the load from both methods using FEKO extracted impedance matrix of wire antenna to test feed points away from the load

central 5th edge. The results for this setup are shown in Figure 6.10. There was not only an increase in magnitude of the mixing frequencies, but also an overall magnitude increase from Figure 6.4 with a central load and feed. This again adds to the assumption that the strategic addition of more time-varying loads provides for an increased density of the current on the antenna while also providing prominent mixing frequency magnitudes as well. The trade-off lies between current magnitude on the antenna and mixing frequency prevalence. The effect of the time-varying loads on the mixing frequency magnitudes was more apparent with the use of multiple loads rather than a single load placed at a different segment from the feed in Figure 6.8. Overall, the results from the FEKO extracted impedance matrix for a wire antenna show good agreement between the Conversion Matrices Method and Landt Integral Method, and gives more intuition to the design of antennas with time-varying loads.

In order to provide an example of a higher f_s that takes a much higher number of mixing frequencies to reach the 0 Hz boundary, the same antenna geometry was used along with new values of $f_s = 80$ MHz and $f_p = 5$ MHz and the feed and load placed back at the center. This allowed for 15 positive and 15 negative mixing frequencies to be evaluated, 31 in total including f_s . Figure 6.11 shows that by

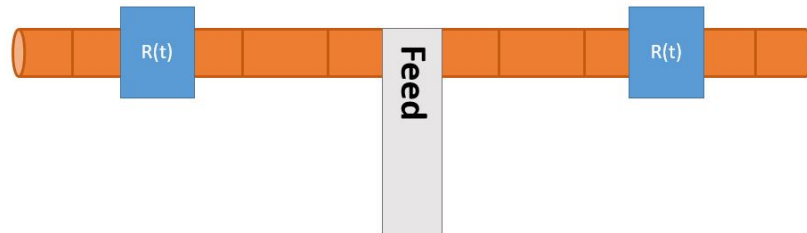


Figure 6.9: Setup of simulation done for FEKO extracted wire antenna impedance matrix to test multiple loads

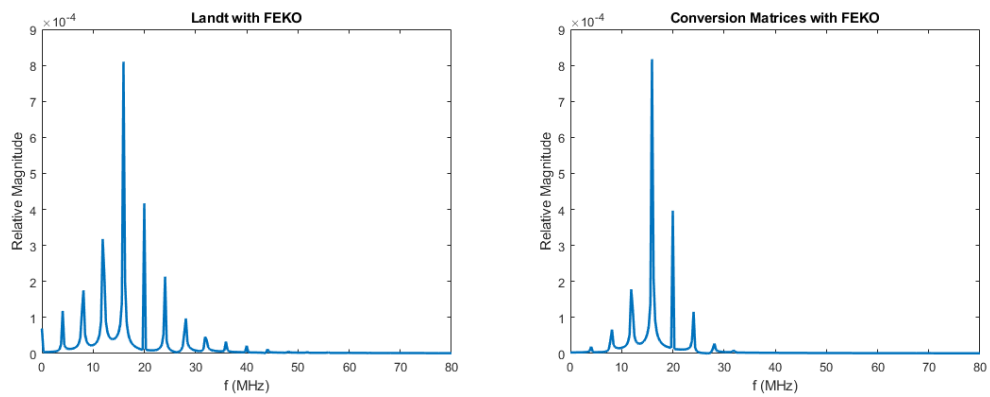


Figure 6.10: Result of current spectrum on the load from both methods using FEKO extracted impedance matrix of wire antenna to test multiple loads

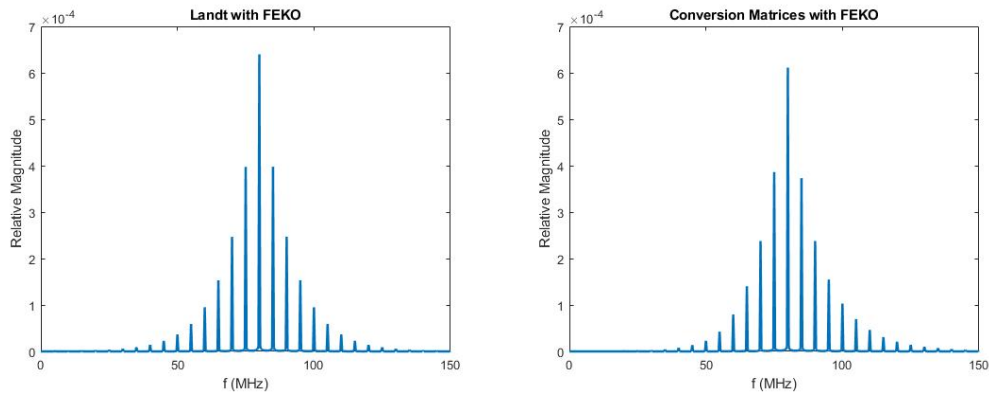


Figure 6.11: Result of current spectrum on wire antenna with higher f_s to avoid 0 MHz, as well as a more refined mesh

shifting the frequencies and allowing for the evaluation of more mixing frequencies, the outer portion of the Conversion Matrices Method spectrum aligns more closely with the Landt Integral Method. It is important to keep the restriction of the zero barrier in mind when using FEKO extracted impedance matrices as it can affect the accuracy of the result. Due to the higher frequency, in order to keep the same accuracy of the solution, FEKO suggested a much more refined mesh, jumping from the 9 segments of the original example, to 37 segments for a “coarse” meshing. While negligible for the Conversion Matrices Method, this increase in impedance matrix size caused a more noticeable jump in the Landt Integral Method run time. For this specific case, the Landt Integral Method ran in 2.986 seconds while the Conversion Matrices Method ran in 1.648 seconds. This was one of the largest gaps in timing seen between the two methods with the Landt Integral Method actually typically running faster for much simpler geometries. It is believed that the benefit of just performing a single matrix multiplication, even if the matrix is much larger like in the Conversion Matrices Method, becomes more efficient than matrix multiplication for each time step if the impedance matrix is large enough.

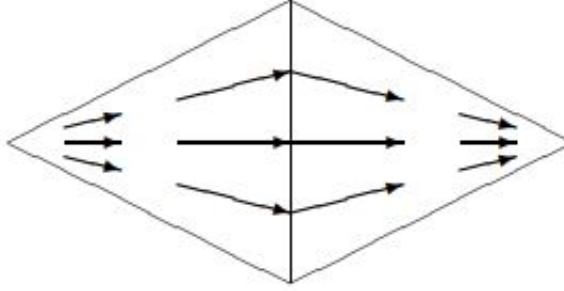


Figure 6.12: Vector plot of RWG basis function from [30]

6.2 Planar Meshing

Once the structure transitions to be two-dimension like a ribbon dipole, the meshing becomes increasingly more complicated. In order to recreate the geometry of a planar structure, simply creating rectangular or square segments is no longer the best or most efficient approach. Triangles are found to be the best at approximating two-dimensional geometries. A basis function using triangular segments was presented by Rao, Wilton, and Glisson in [29], and is referred to as the RWG basis function. The RWG basis function is very similar to the piecewise triangular basis function as it describes the interaction between segments rather than discrete values of a single segment. A visualization of the RWG basis function from [30] is provided in Figure 6.12.

In order to describe the process of planar meshing within FEKO, a ribbon dipole will be used as an example. The first step taken to create the mesh in FEKO is to divide the geometry into a number of triangular segments as described by the RWG basis function. This division can be shown in Figure 6.13.

The ribbon dipole in the example is separated into 8 triangles with 7 edges between them. FEKO then assigns each individual triangle an identification number seen in Figure 6.14. The number assigned to each triangle and the physical points

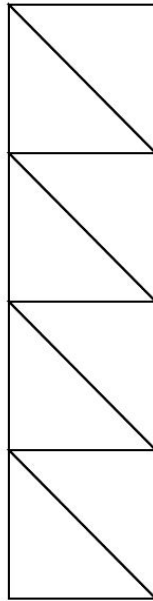


Figure 6.13: Planar mesh of a ribbon dipole

that describe its location are documented in the “.out” file provided by FEKO. Figure 6.15 shows a portion of a real “.out” file extracted from FEKO. This portion shows the number of each of the triangles on the geometry, and the three points that dictate the coordinates of said triangle.

As said before however, FEKO operates using an RWG basis function which focuses instead on the edges between the triangles. This means the elements of the extracted impedance matrix from FEKO for a planar structure describe the impedance between two specified triangles. In the case of the ribbon dipole example provided, in order to center load the dipole, the edge of the two triangles at the center of the dipole must be identified. In Figure 6.16, it can be seen that the center of the dipole lies between triangles 4 and 5. In order to load this edge, the element corresponding to this edge in the impedance matrix can be altered. It can be very difficult however to arbitrarily identify which element in the impedance matrix corresponds to which edge in the mesh when looking at an extracted impedance matrix from FEKO. This

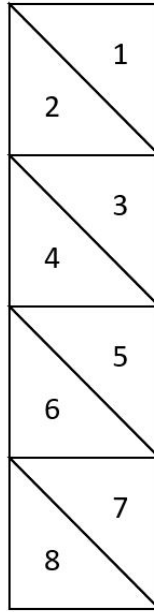


Figure 6.14: Planar mesh with assigned triangle numbers

DATA OF THE METALLIC TRIANGLES

| no. | label | x1 in m | y1 in m | z1 in m | edges | |
|-----|--------|------------|-------------|------------|-------------|----|
| | medium | x2 in m | y2 in m | z2 in m | | |
| | medium | x3 in m | y3 in m | z3 in m | | |
| | | nx | ny | nz | area in m*m | |
| 1 | Union1 | 0.0000E+00 | 2.5000E-01 | 2.0000E+00 | 1 | |
| | Free s | 0.0000E+00 | 2.5000E-01 | 3.0000E+00 | | |
| | Free s | 0.0000E+00 | -2.5000E-01 | 3.0000E+00 | | |
| | | 1.0000E+00 | 0.0000E+00 | 0.0000E+00 | 2.5000E-01 | |
| 2 | Union1 | 0.0000E+00 | 2.5000E-01 | 2.0000E+00 | -1 | 2 |
| | Free s | 0.0000E+00 | -2.5000E-01 | 3.0000E+00 | | |
| | Free s | 0.0000E+00 | -2.5000E-01 | 2.0000E+00 | | |
| | | 1.0000E+00 | 0.0000E+00 | 0.0000E+00 | 2.5000E-01 | |
| 3 | Union1 | 0.0000E+00 | 2.5000E-01 | 1.0000E+00 | 3 | 4 |
| | Free s | 0.0000E+00 | -2.5000E-01 | 0.0000E+00 | | |
| | Free s | 0.0000E+00 | 2.5000E-01 | 0.0000E+00 | | |
| | | 1.0000E+00 | 0.0000E+00 | 0.0000E+00 | 2.5000E-01 | |
| 4 | Union1 | 0.0000E+00 | -2.5000E-01 | 1.0000E+00 | 5 | 6 |
| | Free s | 0.0000E+00 | 2.5000E-01 | 1.0000E+00 | | |
| | Free s | 0.0000E+00 | 2.5000E-01 | 2.0000E+00 | | |
| | | 1.0000E+00 | 0.0000E+00 | 0.0000E+00 | 2.5000E-01 | |
| 5 | Union1 | 0.0000E+00 | -2.5000E-01 | 1.0000E+00 | -2 | -5 |
| | Free s | 0.0000E+00 | 2.5000E-01 | 2.0000E+00 | | |
| | Free s | 0.0000E+00 | -2.5000E-01 | 2.0000E+00 | | |
| | | 1.0000E+00 | 0.0000E+00 | 0.0000E+00 | 2.5000E-01 | |
| 6 | Union1 | 0.0000E+00 | 2.5000E-01 | 1.0000E+00 | -3 | -6 |
| | Free s | 0.0000E+00 | -2.5000E-01 | 1.0000E+00 | | |
| | Free s | 0.0000E+00 | -2.5000E-01 | 0.0000E+00 | | |

Figure 6.15: Portion of real “.out” file from FEKO describing triangles

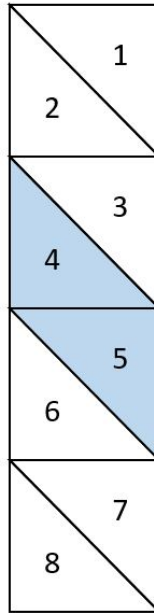


Figure 6.16: Planar mesh edge being identified

is why it is important to once again look at the “.out” file for guidance. The first step is to determine the two triangles that correspond to the physical location to be loaded. These triangle numbers can be identified from the portion of the “.out” file shown in Figure 6.15. Once the triangles for the physical location of the load are identified, the number of the edge between them must be found. Figure 6.17 shows an example of the edge information from the “.out” file. Each number is the individual edge between two triangles identified by the variables *KORP* and *KORM*. In this specific “.out” file, it can be seen that the edge 6 is between triangles 4 and 6. Once the edge number is identified, that number is the corresponding element number of the load location in the FEKO extracted impedance matrix.

DATA OF THE METALLIC EDGES (with MoM)

| no. | type | length/m | media | | triangle no. | | points of tr. | | information on symmetry | | | status |
|-----|------|------------|--------|----|--------------|------|---------------|------|-------------------------|----|----|---------|
| | | | | | KORP | KORM | POIP | POIM | yz | xz | xy | |
| 1 | 1 | 1.1180E+00 | Free s | -1 | 1 | 2 | 2 | 3 | 0 | 0 | 0 | unknown |
| 2 | 1 | 5.0000E-01 | Free s | -1 | 2 | 5 | 2 | 1 | 0 | 0 | 0 | unknown |
| 3 | 1 | 1.1180E+00 | Free s | -1 | 3 | 6 | 3 | 2 | 0 | 0 | 0 | unknown |
| 4 | 1 | 5.0000E-01 | Free s | -1 | 3 | 9 | 1 | 1 | 0 | 0 | 0 | unknown |
| 5 | 1 | 1.1180E+00 | Free s | -1 | 4 | 5 | 2 | 3 | 0 | 0 | 0 | unknown |
| 6 | 1 | 5.0000E-01 | Free s | -1 | 4 | 6 | 3 | 3 | 0 | 0 | 0 | unknown |
| 7 | 1 | 1.1180E+00 | Free s | -1 | 7 | 8 | 2 | 3 | 0 | 0 | 0 | unknown |
| 8 | 1 | 5.0000E-01 | Free s | -1 | 8 | 11 | 2 | 1 | 0 | 0 | 0 | unknown |
| 9 | 1 | 1.1180E+00 | Free s | -1 | 9 | 12 | 3 | 2 | 0 | 0 | 0 | unknown |
| 10 | 1 | 1.1180E+00 | Free s | -1 | 10 | 11 | 2 | 3 | 0 | 0 | 0 | unknown |
| 11 | 1 | 5.0000E-01 | Free s | -1 | 10 | 12 | 3 | 3 | 0 | 0 | 0 | unknown |

Figure 6.17: Portion of real “.out” file from FEKO describing edges between triangles

6.2.1 Ribbon Dipole

As was stated in the planar meshing section, a ribbon dipole is one of the simplest planar geometries to be observed. In the design in FEKO, the ribbon dipole was assumed to be infinitely thin and was created with a 2D rectangle. It was seen as more important to focus on the meshing of the planar dimension before accounting for plane thickness. In order to test the behavior of the Conversion Matrices Method on planar components, a ribbon dipole was made by creating a plane $4.5m \times 0.2m$. This ribbon dipole was separated into 12 metallic triangles with 11 edges shown in Figure 6.18.

The setup for the first base results was very similar to that of the wire dipole. The ribbon dipole was centrally fed and loaded as shown in Figure 6.19. Identifying the central edge however was more complicated than for the thin wire dipole. The edges were no longer just the vertical edges across the wire antenna, but also the diagonal edges between triangles. The “.out” file of the antenna extracted from FEKO can then be used to identify which element of the impedance matrix corresponds to which edge. For this specific meshing, the central edge was between triangles 6 and 12 and the edge number was 6. The numbering of the triangles and edges are

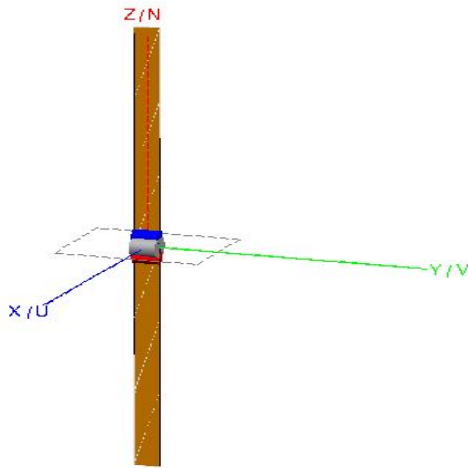


Figure 6.18: Simulated model in FEKO for ribbon dipole, separated into 12 triangles with 11 edges between them

shown in Figure 6.20. This shows that the process and numbers assigned to each triangle and edge is not as intuitive as the segmented thin wire antenna.

The results for current spectrum of this base example are shown in Figure 6.21. The spectrums show good agreement; however, it is apparent that Landt Integral Method is not computed with a finite number of mixing frequencies while the Conversion Matrices Method is. The overall distribution and magnitude of the spectrums are very similar between the two methods, giving confidence that the method could be translated to planar structures. The discrepancies are primarily shown towards the outer edges of the spectrum which was expected with the zero boundary limiting the number of mixing frequencies the Conversion Matrices Method can analyze. In order to confirm this planar model was fully compatible with the Conversion Matrices Method, tests for different case scenarios were performed on the FEKO extracted planar impedance matrix.

The first case was moving the feed and load at a point away from the center of the antenna. This was to verify that the methods agreed when the loading and

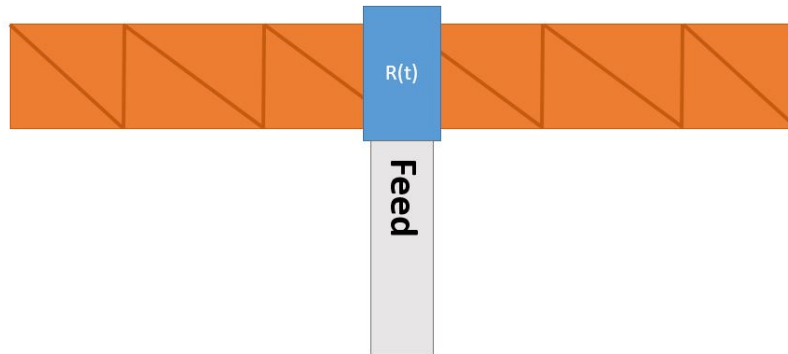


Figure 6.19: Setup of simulation done for FEKO extracted ribbon dipole impedance matrix with load and feed at center



Figure 6.20: Triangle and edge numbers in meshing identified from FEKO “.out” file

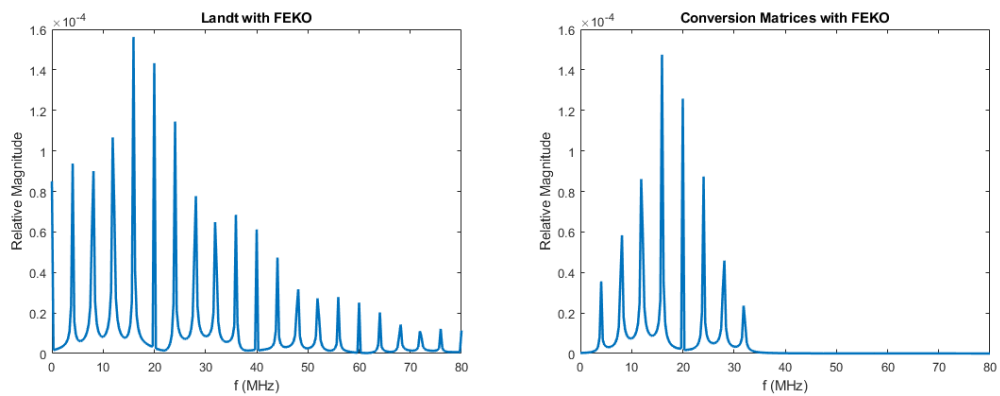


Figure 6.21: Results of the current spectrum on the central load from the Landt Integral Method and Conversion Matrices Method using a FEKO extracted impedance matrix of a ribbon dipole

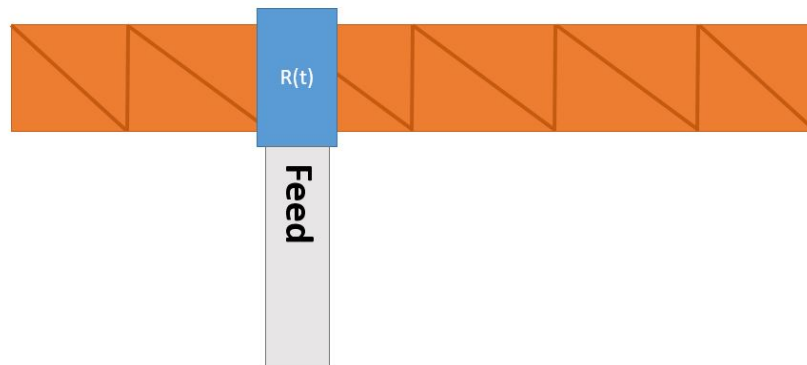


Figure 6.22: Setup of simulation done for FEKO extracted ribbon dipole impedance matrix with load and feed at edge 10, away from the center

feeding point were moved to different elements in the impedance matrix. The load and feed were moved to the next straight segment over from the center, which was the edge connecting triangles 9 and 10. This edge was labeled as 10, dictating its element number in the extracted impedance matrix. The setup of this case is shown in Figure 6.22. The results for this setup are shown in Figure 6.23. The results are very similar to that of Figure 6.21; however, with a decrease in the overall magnitude. This is expected as the feed and load are being moved away from the current maximum of the center.

The second case was testing a feed location at a different location from the load. This was done to ensure that the capability to observe the current on the antenna at locations different from the load still worked for planar structures. The setup for this example is shown in Figure 6.24, and the results shown in Figure 6.25 show that the magnitudes of the mixing frequencies are almost entirely diminished by the feed being two edges (or one vertical edge) away from the load. This does make sense as this is a separation of about 0.75 m physically. The fairly abrupt decrease in mixing frequency level as the feed moves away from the time-varying load has

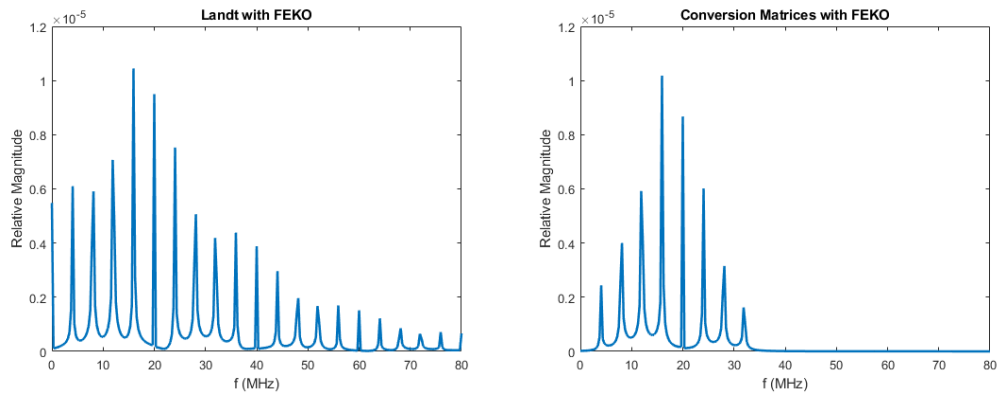


Figure 6.23: Results of the current spectrum on the off-center load from the Landt Integral Method and Conversion Matrices Method using the FEKO extracted impedance matrix of a ribbon dipole

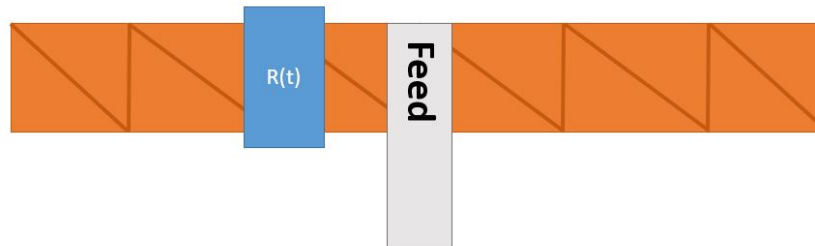


Figure 6.24: Setup of the simulation in FEKO for the extracted ribbon dipole impedance matrix with load at edge 10 and feed at the center

been consistent throughout the entirety of this thesis.

The planar structure was then tested for its ability to handle the addition of multiple loads. In order to test this, a second load was added to the other side of the central feed proportionally the same distance as the first load. The setup for this final example is shown in Figure 6.26. The results in Figure 6.27 shown not only an increase in magnitude of the mixing frequencies from Figure 6.24, but also greater spectral spreading. This is very similar to the results of the addition of a secondary load in Figure 6.10. Overall, there is great agreement between the Landt Integral Method and Conversion Matrices Method.

Finally, the same higher frequency example from the wire dipole was applied to

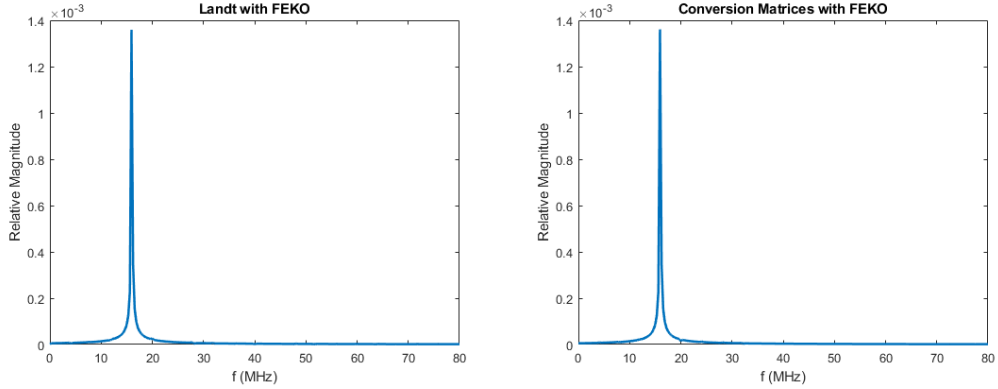


Figure 6.25: Results of the current spectrum for the off-center load and center feed for the Landt Integral Method and Conversion Matrices Method using the FEKO extracted impedance matrix of a ribbon dipole

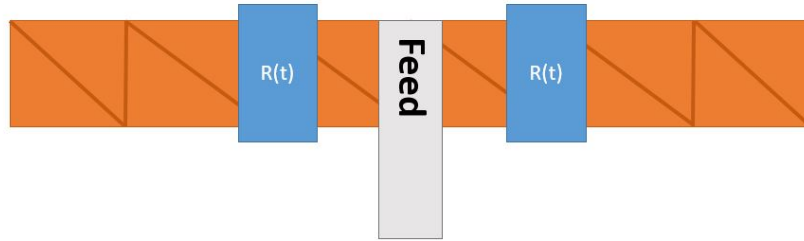


Figure 6.26: Setup of the simulation done in FEKO for the extracted ribbon dipole impedance matrix with multiple loads

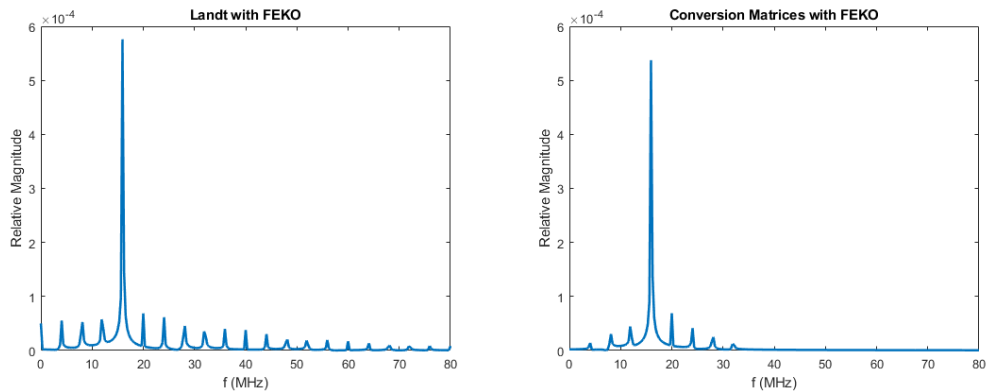


Figure 6.27: Results of the current spectrum in the center of two loads from the Landt Integral Method and Conversion Matrices Method using the FEKO extracted impedance matrix of a ribbon dipole

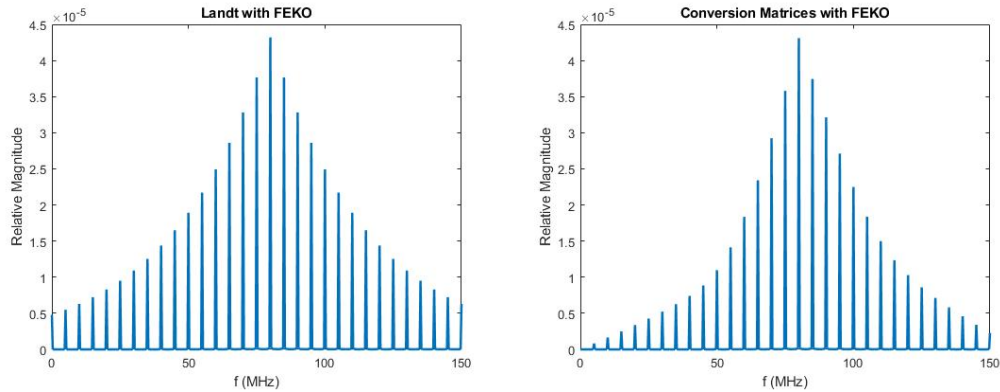


Figure 6.28: Result of the current spectrum on a planar antenna with a higher f_s to avoid 0 MHz, as well as a more refined mesh

the geometry of the ribbon dipole to test the agreement between the two methods with a higher number of mixing frequencies. The frequency values were changed to $f_s = 80$ MHz and $f_p = 5$ MHz, and the feed and load were placed at the center. The results in Figure 6.28 show that with a higher number of mixing frequencies, the outer portion of the spectrum between the two methods match up better. In order to account for the higher frequency, the “coarse” mesh in FEKO required significantly more triangles, moving from 12 to 139. This large increase in the impedance matrix size was very apparent in the computation time. The Conversion Matrices Method took 5.943 seconds to run, while the Landt Integral Method made the jump to 106.477 seconds. This further builds the idea that the Conversion Matrices Method will be a much more efficient computation method when the geometries of the antenna become increasingly more complicated, resulting in more intricate meshing and therefore larger impedance matrices.

6.3 Summary

The Conversion Matrices Method has shown to be compatible with the extracted FEKO impedance matrices, which provides a more generalized application of the method. While there are slightly more discrepancies between the CMM and Landt Integral Method using FEKO impedance matrices, there is still great agreement between the two methods. More work needs to be done on a wider variety of antennas such as loops and larger planar structures like patch antennas. By creating this generalization, it is believed that the characterization of time-varying loads on antennas can be done in an efficient manner, and this technique will be a useful tool in encouraging further research of such antennas.

Chapter 7

Conclusions and Future Work

The application of time-varying loads has been observed on a variety of components for a variety of reasons. Time-varying loads have been shown to model effects of parametric amplification such as frequency conversion, and in some cases are used to create a nonreciprocity in both filters and transmission lines. This project sought to utilize time-varying loads to break the Linear Time-Invariant (LTI) assumption made of most antennas, and utilize their effects to bypass the performance limitations on electrically small antennas set by [2]. One of the main concerns with the application of time-varying loads is the methods with which to model them. Many typical methods rely on the same LTI assumption. This thesis presented a generalized and extended frequency domain method for modeling time-varying loads on antennas using a combination of method of moments and conversion matrices called the Conversion Matrices Method.

While methods using conversion matrices have been presented before for this application, they have relied on the use of a single equivalent circuit to model the antenna. This presents two main issues: the inability to observe the currents on the antenna at locations differing from the load and model multiple time-varying loads on the antenna. The extension of this method by applying conversion matrices to the entirety of the impedance matrix of an antenna extracted using method

of moments provides a solution for both of the aforementioned limitations. This method has been shown to have great agreement with the time stepping method for analyzing time-varying loads called the Landt Integral Method. In order to make the method capable of modeling arbitrary antenna shapes, it was modified to be applied to impedance matrices extracted from an electromagnetic solver that uses method of moments. In this thesis, the FEKO software package was chosen to extract said impedance matrices. Method of moments impedance matrix solutions can become increasingly difficult to calculate by hand as the geometry becomes more complicated, and the use of FEKO allows for that difficulty to be bypassed.

The work on this project however is far from done. The steps to be taken in future work can be separated into two main categories, expansion and validation. The first category, expansion, refers to the addition of techniques to be implemented with the Conversion Matrices Method. One important addition is the method of harmonic balance. All the loads in this thesis were assumed to be linear and time-varying, and conversion matrices are defined by [23] to be the secondary portion of small/large signal analysis after harmonic balance is performed. By applying harmonic balance solutions to the method, it would expand the method to be applicable with nonlinear components, such as varactors, in addition to time-varying components.

The second category for future work is validation, which would ideally be done with two methods. The first of which is through a standardized time-domain electromagnetic solver called XFDTD which uses finite difference time-domain. Being able to compare results to software that is commercially available is seen as a good next step in the direction of further validating the Conversion Matrices Method. Once this validation can be made, antennas with time-varying loads can be fabricated and tested for real physical measurements. The validations made before this

final step however are incredibly important in order to avoid unnecessary design mistakes, as this type of antenna does not have a wide range of general antenna knowledge or intuition that can be applied.

Overall, this thesis has provided a basis for the further development of the Conversion Matrices Method. It has shown the method is a very promising frequency domain alternative to the time domain methods that dominate nonlinear and time-varying load modeling. The method has been generalized to be applied with electromagnetic computation software such as FEKO, and it is believed that continued work will provide a prominent and efficient alternative to simulation in the growing field of nonlinear and time-varying antennas.

References

- [1] H. A. Wheeler, “Fundamental limitations of small antennas”, *Proceedings of the IRE*, vol. 35, no. 12, pp. 1479–1484, 1947.
- [2] L. J. Chu, “Physical limitations of omni-directional antennas”, *Journal of applied physics*, vol. 19, no. 12, pp. 1163–1175, 1948.
- [3] R. Collin and S. Rothschild, “Evaluation of antenna Q”, *IEEE Transactions on Antennas and Propagation*, vol. 12, no. 1, pp. 23–27, 1964.
- [4] J. S. McLean, “A re-examination of the fundamental limits on the radiation Q of electrically small antennas”, *IEEE Transactions on antennas and propagation*, vol. 44, no. 5, p. 672, 1996.
- [5] S. R. Best, “A discussion on the quality factor of impedance matched electrically small wire antennas”, *IEEE Transactions on Antennas and Propagation*, vol. 53, no. 1, pp. 502–508, 2005.
- [6] E. Nordholt and D. Van Willigen, “A new approach to active antenna design”, *IEEE Transactions on Antennas and Propagation*, vol. 28, no. 6, pp. 904–910, 1980.
- [7] J. Hopf and H. Lindenmeier, “Fast tunable active receiving antennas”, *Radio Science*, vol. 16, no. 6, pp. 1143–1147, 1981.
- [8] A. Bahr, “On the use of active coupling networks with electrically small receiving antennas”, *IEEE Transactions on Antennas and Propagation*, vol. 25, no. 6, pp. 841–845, 1977.
- [9] P. Loghmannia and M. Manteghi, “A parametric amplifier slot antenna”, in *2018 IEEE International Symposium on Antennas and Propagation & USNC/URSI National Radio Science Meeting*, IEEE, 2018, pp. 487–488.
- [10] K. Schab, D. Huang, and J. J. Adams, “Pulse characteristics of a direct antenna modulation transmitter”, *IEEE Access*, 2019.

- [11] Q. X. Shihan Qin and Y. E. Wang, “Nonreciprocal components with distributedly modulated capacitors”, *IEEE Transactions on Microwave Theory and Techniques*, vol. 62, no. 10, pp. 2260–2272, Oct. 2014, ISSN: 0018-9480. DOI: 10.1109/TMTT.2014.2347935.
- [12] X. Wu, X. Liu, M. D. Hickle, D. Peroulis, J. S. Gómez-Díaz, and A. Á. Melcón, “Isolating bandpass filters using time-modulated resonators”, *IEEE Transactions on Microwave Theory and Techniques*, vol. 67, no. 6, pp. 2331–2345, 2019.
- [13] L. A. Blackwell and K. L. Kotzebue, “Semiconductor-diode parametric amplifiers”, 1961.
- [14] M. Kanda, “Analytical and numerical techniques for analyzing an electrically short dipole with a nonlinear load”, *IEEE Transactions on Antennas and Propagation*, vol. 28, no. 1, pp. 71–78, 1980.
- [15] R. Luebbers, J. Beggs, and K. Chamberlin, “Finite difference time-domain calculation of transients in antennas with nonlinear loads”, *IEEE transactions on antennas and propagation*, vol. 41, no. 5, pp. 566–573, 1993.
- [16] T. Liu and F. Tesche, “Analysis of antennas and scatterers with nonlinear loads”, *IEEE Transactions on Antennas and Propagation*, vol. 24, no. 2, pp. 131–139, 1976.
- [17] J. Landt, E. Miller, and F. Deadrick, “Time domain modeling of nonlinear loads”, *IEEE Transactions on Antennas and Propagation*, vol. 31, no. 1, pp. 121–126, 1983.
- [18] J. Landt, “Network loading of thin-wire antennas and scatterers in the time domain”, *Radio Science*, vol. 16, no. 6, pp. 1241–1247, 1981.
- [19] ———, “Effects of nonlinear loads on antennas and scatterers”, *AGAARD Lecture Series*, vol. 131, 1983.
- [20] R. F. Harrington, *Field computation by moment methods*. Wiley-IEEE Press, 1993.
- [21] A. Kerr, “A technique for determining the local oscillator waveforms in a microwave mixer (short papers)”, *IEEE Transactions on Microwave Theory and Techniques*, vol. 23, no. 10, pp. 828–831, 1975.

- [22] C.-C. Huang and T.-H. Chu, “Analysis of wire scatterers with nonlinear or time-harmonic loads in the frequency domain”, *IEEE transactions on antennas and propagation*, vol. 41, no. 1, pp. 25–30, 1993.
- [23] S. A. Maas, *Nonlinear microwave and RF circuits*. Artech house, 2003.
- [24] F. De Flaviis, R. Coccioli, and T. Itoh, “Nonlinear analysis and evaluation of distortion introduced by micro electromechanical switches in reconfigurable antenna systems”, in *Proc. AP2000, Millennium Conf. Antennas Propagat*, 2000, pp. 9–14.
- [25] W. C. Gibson, *The method of moments in electromagnetics*. Chapman and Hall/CRC, 2007.
- [26] S. J. Orfanidis, “Electromagnetic waves and antennas, 2008”, *Unpublished*, available: <http://www.ece.rutgers.edu/orfanidi/ewa>, 2004.
- [27] S. A. Maas, “Microwave mixers”, *Norwood, MA, Artech House, Inc., 1986*, 368 p., 1986.
- [28] J. Stewart, *Calculus: Concepts and contexts*. Cengage Learning, 2009.
- [29] S. Rao, D. Wilton, and A. Glisson, “Electromagnetic scattering by surfaces of arbitrary shape”, *IEEE Transactions on antennas and propagation*, vol. 30, no. 3, pp. 409–418, 1982.
- [30] D. B. Davidson, *Computational electromagnetics for RF and microwave engineering*. Cambridge University Press, 2010.